Strength of Grass Covers on Dikes

R.J. Wegman

TU Delft Delft University of Technology

INFRAM HYDREN Hydraulic Engineering, Innovation & Research

Strength of Grass Covers on Dikes

by

R.J. Wegman

in partial fulfillment of the requirements for the degree of

Master of Science
in Civil Engineering

at the Delft University of Technology (TU Delft),
to be presented publicly on Monday February 10, 2020 at 14:00.

Student number :	4523822	
Thesis committee	Prof. dr. ir. S.G.J. Aarninkhof	TU Delft, Section Coastal Engineering
	Dr. ir. M. van Damme	TU Delft, Section Hydraulic Structures and Flood Risk
	Dr. ir. G.H. Keetels	TU Delft, Department Maritime & Transport Technology, Section Offshore & Dredging Engineering
	Ir. G.J. Steendam	Infram Hydren
	Ir. R.J.C. Mom	Infram Hydren

TU Delft Delft University of Technology

INFRAM HYDREN Hydraulic Engineering, Innovation & Research

Preface

This master thesis marks the end of my time as a student. This time was characterised by acquiring new knowledge, making new friends and discovering new worlds. After gaining all these experiences and hard work, I'm happy to present my graduation work on the strength of grass covers on dikes.

This research is a continuation of a longer sequence of studies that have been conducted at the Delft University of Technology in cooperation with Infram Hydren. I am glad I had the possibility to contribute to this ongoing research. However, without help this would not have been possible. Therefore I would like to thank my supervising committee for their advice and feedback. Many thanks to Myron van Damme, for your limitless time and valuable knowledge. You helped me to create my research and to structure my writing process. Many thanks to Gosse Jan Steendam, Roy Mom and Jan Bakker for sharing your knowledge and practical expertise. Furthermore, I would like to thank Stefan Aarninkhof and Geert Keetels for your valuable feedback. The meetings with the committee provided valuable insights that enabled me to improve my graduation work. Moreover, this research was not possible without the test locations provided by Waterschap Drents Overijsselse Delta and Wetterskip Fryslân and the support of Infram Hydren to enable the field experiments.

I would like to thank my colleagues of Infram Hydren and the GOS team for all enjoyable moments during the last year, it is a pleasure to work with you! But most of all, I would like to thank my family and friends for your moral support and company.

Rik Wegman
Den Hoorn, January 2020

Abstract

Wave overtopping is responsible for many dike failures, dike breaches and severe flooding. The erosion resistance of dikes to overtopping waves is determined by the strength of the grass cover. Therefore, a thorough understanding of the erosion resistance of grass covers is desired to enable a good and effective dike management. In the existing approach to assess the erosion resistance of grass covers, the erosion resistance is empirically quantified in terms of local hydraulic loads. However, despite the cyclical nature of overtopping waves, no insights into the dependence of the erosion resistance on successive loads are available.

To improve the understanding of the resistance of grass covers to wave overtopping induced loads, understanding of the development of the mechanical behaviour of grass sods is essential. In this study the mechanical behaviour of grass covers under tensile loads have been examined by means of direct pull tests executed in the field. Especially the influence of repetitive wave loading and the conditions during testing were of interest.

The results of this study show that the deformation of the grass cover due to tensile load is time dependent. The failure mode of the grass cover is influenced by the degree of saturation of the grass cover. The maximum strength and mechanical behaviour of the grass cover is influenced by accumulation of damage. The findings presented in this study provide a better understanding of the processes that influence the mechanical behaviour of the grass cover. Moreover, insights in the development of the process of damage accumulation are revealed.

Based on the findings of this study, a method is proposed to determine the resistance of grass covers against repetitive loads by means of direct pull tests. In this method the resistance of grass covers against repetitive loads is described by an estimation of the fatigue limit. Relating the fatigue limit of a grass cover to hydraulic loads, enables an assessment of the erosion resistance of a grass cover at a specific location.

Contents

1

Introduction

Worldwide a large and rising number of people live in low laying coastal and river areas. By 2070, most likely 140 million people and 30.000 billion euro of assets depend on flood protection in large port cities only (Kok et al., 2013). Large coastal areas are protected against flooding by man-made dikes. Just looking at the Netherlands, two-thirds of the country would be endangered by flooding without dikes (Takken et al., 2009). Consequently, flood protection is of enormous importance. In the past, wave overtopping has been responsible for many dike failures, dike breaches and severe floodings (Schüttrumpf and Van Gent, 2003; Van der Meer et al., 2006). According to Kortenhaus (2003), wave overtopping is one of the main causes of dike failure. To protect dikes against wave overtopping, the majority of the river and sea dikes in the Netherlands are covered with grass. Once the grass cover has eroded, the core of the dike is exposed to wave action and starts to erode, possibly resulting in a dike breach. Therefore it is assumed that the erosion resistance of dikes is determined by the strength of the grass cover (Verheij et al., 1997).

1.1. Background

Wave attack occurs during an extreme event with high water levels and high waves. Breaking waves run up the slope of the dike, and the highest waves overtop the dike. Wave attack runs through several stages. In Figure 1.1, the different processes during wave attack on the dike are depicted. Based on the nature of the flow characteristics, the dike has been divided in four different parts (Schüttrumpf and Oumeraci, 2005).

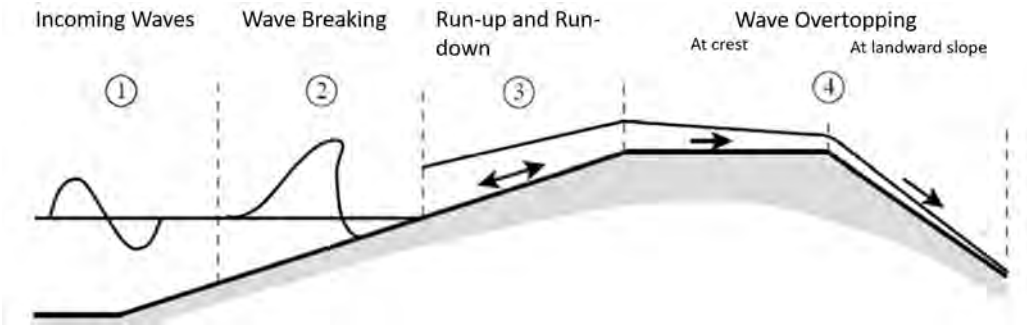

Figure 1.1: Hydraulic processes of breaking, run-up and run-down and overtopping of waves. Reprinted from Schüttrumpf and Oumeraci (2005).

In general, Dutch sea dikes consist of a sand core enclosed by a layer of clay. Because of the nature of the forces induced by wave breaking and economical considerations, only the lower part of the seaward slope is provided with expensive hard protections. The cover layer on the upper part of the seaward slope, the crest and landward side is protected by a grass cover layer. River dikes are usually completely covered with a grass cover on the crest and on both the inner and outer slope. Frequent wave run-up and wave overtopping induce loads on the grass cover which result in erosion.

The flow characteristics of overtopping wave are well studied (Schüttrumpf and Oumeraci, 2005; Schüttrumpf and Van Gent, 2003). To gain insight in the complex processes of the effect of overtopping waves on grass cover, extensive research has been carried out during the last decades. To simulate the overtopping waves and test the strength of dike covers, a mobile full scale simulator was developed and designed within the ComCoast project (Van der Meer et al., 2006; Van Der Meer et al., 2007).

Failure mechanisms of grass covers
The results of various field experiments with the wave overtopping simulator have lead to the description of different mechanisms of failure or erosion of the grass cover. A distinction is made between the erosion processes that cause failure of the grass cover and the type of failure of the slope (Ponsioen, 2016). 'Technisch rapport toetsen grasbekledingen op dijken' (Van der Meer et al., 2012) describes the different erosion processes of the grass cover as explained below.

Pull-out mechanism.
The pull-out mechanism is observed at the onset of grass cover dislocation (Van der Meer et al., 2012), the occurrence of the pull-out mechanism can result in other mechanisms. The flow lifts a part of the sod and pulls it out of the soil structure. Initially bulging or complete pull-out of the sod occurs. The flow will eventually tear the lifted part out of the sod. Typical dimensions of removed sod due to pull-out is 15 cm x 15 cm to 50 cm x 50 cm (Van der Meer et al., 2012) . This mechanism can just remove thin layer of the sod, but also complete removal of the sod is observed.

Jet erosion.
Jet erosion occurs mainly on transitions of flow direction and velocity. Especially around the toe of the dike (Valk, 2009). In recent research the same process was observed at the transition of the dike crest to the land side slope (Ponsioen, 2016; Van Damme et al., 2016). The overtopping waves separate from the surface at the transition of the dike crest to the land side slope, this causes a large impact and creates a hole in the grass cover.

Wear Erosion.
Wear erosion is the transport of particles by the water flow during wave overtopping. Due to a lack of cohesion within the grass cover, the water flow is able to erode clay particles piecewise during succeeding wave cycles (Van der Meer et al., 2012).

After initiation of failure due to erosion processes, even more complex processes are initiated that eventually can lead to failure of the slope (Bijlard, 2015). Hai and Verhagen (2014) distinguish three failure mechanisms of the grass cover: roll-up, head-cut and collapse. Roll-up damage is induced when the flow lifts the turf and pushes it over. After initiation, the grass sod is slowly pulled down along the slope. The grass cover characteristics influence the occurrence of roll-up damage. Head-cut damage is the simultaneous removal of the turf and the clay layer, hence lifting of the soil. After initiation of first damage to the grass cover, damaged spots are enlarged in both area and depth. The clay layer on the slope is undermined and an erosion hole with relatively vertical walls develops. Head-cut erosion is explained by a local weak spot at depth. The occurrence of this failure mechanism, largely depends on the composition of the soil body. Collapse type of damage is observed at dikes predominantly consisting of non-cohesive sandy material. Once initial damage reaches the sandy core, the sand erodes at a large speed and the cover is undermined and collapses. Another type of failure is sliding of large parts of the grass cover, due to an decrease in shear strength of the grass cover (Valk, 2009).

Load mechanisms by overtopping waves
In the existing empirical approach to determine the load imposed by overtopping waves, local hydraulic loads in combination with the observed failure mechanisms are used to explain failure of the grass cover. The roughness of the surface causes the overtopping flow to induce shear stress to the surface (Schiereck, 2012). The shear stress results in force parallel to the slope (Van Damme, 2016). In addition to the force parallel to the slope, Van Langevelde (2017) describes in his Master thesis secondary effects due to the interaction of the shear stress and the grass sod. According to Van Langevelde (2017), this interaction can be compared with the effect of a pushing force perpendicular to the slope in the first part of the wave front and the effect of a lifting force perpendicular to the slope in the second part of the wave front.

According to the cumulative overload method, developed by Van der Meer et al. (2010), the onset of failure is related to peak loads in shear stresses induced by the overtopping wave. This relation is based on an empirical relation between the peak wave front flow velocity and damage to the grass cover due to erosion. It is assumed that only loading above a threshold value contributes to erosion of

the grass cover.

The second load mechanism considers pressure fluctuations in turbulent flow. During wave overtopping, turbulence appears in the overtopping flow and results in a considerable amount of pressure fluctuations. The dynamic pressure can be directed both upward and downward. Measurements showed that negative pressure perpendicular to the grass cover causes a lift force during wave overtopping (Hoffmans, 2012; Verheij et al., 2015). Dynamic pressure is observed at the onset of slope dislocation (Hoffmans, 2012).

The third load mechanism is loading by wave impact. Wave impact or jet impact occurs mainly on transitions of flow direction and velocity (Ponsioen et al., 2019; Valk, 2009; Van Damme et al., 2016). The impact stress can be decomposed in an impact stress component parallel to the slope and an impact stress component perpendicular to the slope. This results in compression and shear loading of the grass cover. Van Langevelde (2017) concludes that none of the described loading mechanisms is all-embracing and none of them excludes all others. This indicates that multiple mechanisms can occur simultaneously.

Strength of the grass cover
In line with the existing empirical approach to determine the load imposed by overtopping waves, local hydraulic loads are used to empirically quantify the erosion resistance of grass covers subject to overtopping waves. According to the cumulative overload method, only loading above a threshold value of local hydraulic loads contributes to erosion of the grass cover (Van der Meer et al., 2010). Therefore this threshold value, the critical wave front peak flow velocity u_c, is used to empirically quantify the erosion resistance of grass covers subject to overtopping waves. Within the cumulative overload method, u_c is assumed to be constant over time, regardless the load history of the grass cover. By executing tests with the wave overtopping simulator it is possible to determine critical flow velocity as a measure of the erosion resistance of the grass cover at that specific location. However, it appeared to be difficult to quantify u_c. The Cumulative Overload Method is described in more detail in Appendix A.

Besides the wave overtopping simulator, a device was developed by Infram B.V. in cooperation with Van der Meer Inovations to investigate the strength of grass covers on dikes. This device, named the grass pulling device, aims to measure the strength of the grass sod in situ. While lifting the grass sod perpendicular out of the grass cover, the imposed force is measured. This device is originally developed to fit the Cumulative Overload Method developed by Van der Meer et al. (2010), rather than mimic the load induced by overtopping waves. However, the lifting of the sod is in line with part of the load mechanisms induced to overtopping waves. Bijlard (2015; 2017) used the Turf-element model (Hoffmans et al., 2009) to find a relation to express the maximum lifting force found with the grass pulling device into the critical flow velocity that can be used as indication of the strength of the grass cover of the dike. This method is described in more detail in Appendix B.

1.2. Problem description

For a good and effective dike management a thorough understanding of the erosion resistance of grass covers is desired. During the last decades a substantial amount of studies were preformed to illuminate the erosion process of grass covers on dikes. This research provides insights in the different failure mechanisms of a grass cover due to overtopping waves. The existing empirical approach used to relate local hydraulic loads to observed failure mechanisms, enables to empirically quantify the erosion resistance of grass covers subject to overtopping waves in terms of local hydraulic loads (Van der Meer et al., 2010).

This empirical approach, the cumulative overload method, shows predictive value (Bomers, 2015; Steendam et al., 2014). However, evaluation of this method has highlighted two problems. First, threshold value u_c required for these methods is difficult to quantify (Ponsioen et al., 2019). Second, u_c is assumed to be constant over time. It is however not possible to determine the effect of a single wave to the strength of the grass cover during wave overtopping tests. It is only possible to determine the erosion resistance of the grass cover after damage to the grass cover has occurred. Hereby, no insight in the development of the erosion resistance during a test with the wave overtopping simulator is gained. To improve the understanding of resistance of grass covers to wave overtopping induced loading, understanding of the mechanical behaviour of grass sods is essential. Bijlard (2015; 2017) made a start revealing the mechanical characteristics of grass sod. However, still a great deal of the

mechanical characteristics is unknown.

Besides the state-of-the-art empirical approach, theoretical approaches to reveal the physical processes during wave overtopping are subject of ongoing research. Because of the difficulties to determine the stresses in the grass cover during wave overtopping tests, attempts were made to model the combination of hydraulic loads and stress development in the grass cover based on theoretical models, e.g. based on continuum behaviour of porous media (Van Damme, 2019) or discrete element model describing particle-particle interactions as described by Helmons and Van Rhee (2019). In these approaches, the behaviour of the grass cover is modelled based on the mechanical characteristics of the grass cover. Utilisation of this theoretical approaches desires a more detailed description of the material characteristics of the grass cover.

To narrow the scope of this research, measurements were executed in the preliminary phase of this researched to indicate the strength of the grass cover. During the test, the grass sod with a surface area of $20 \times 20\,cm^2$ was lifted from the grass cover and the grass sod with a surface area of $20 \times 20\,cm^2$ was sheared parallel to the slope. The results of this measurement showed that the strength of the grass sod in parallel direction to the slope is a great deal larger than the strength in perpendicular direction to the slope. In addition to the indication of the strength magnitude, this tests identified practical problems during execution of the tests to measure the strength parallel to the slope. Due to dilation of the grass cover, it appears almost impossible to execute this tests up to failure of the grass sod due to loading parallel to the slope.

1.3. Research questions and objectives

In this thesis, the strength of the grass cover of dikes was studied. Attempts were made to formulate a method to reveal the mechanical behaviour of the grass sod. The material behaviour of grass sods is essential in understanding the resistance of grass covers to loading by overtopping waves. The prevailing knowledge on the interaction between overtopping waves and grass covers on dikes, shows that, combining the typical strength of grass covers and the typical load induced by overtopping waves, the grass cover is most vulnerable to the lift force perpendicular to the slope. This is supported by the observation during wave overtopping simulation tests. In case of a well developed grass cover, the pull-out mechanism is observed at the onset of failure grass cover. For this purpose, the tensile strength of a grass cover is investigated in the field by means of direct pull tests with a grass pulling device as described by Bijlard (2015; 2017). Especially the influence of repetitive wave loading and the conditions during testing are of interest. The main purpose of this research is formulated in the following objective:

Improve the understanding of the mechanical behaviour of grass covers.

In order to answer this objective, the following research questions were defined:

1. What are the physical processes and associated parameters that provide resistance of the grass cover against pull-out erosion induced by overtopping waves?
2. What method can be used to measure the strength parameters?

The following deliverables will help in achieving the main objective:

1. The design and execution of field experiments in which the influence of physical processes on the machanical behaviour of the dike cover is determined.
2. A description of the material behaviour of grass covers.
3. Recommendations to improve the method to determine the strength parameters of the grass cover.

1.4. Thesis outline

In order to answer the research questions and to fulfil the objectives presented above, three research phases are distinguished in this thesis:

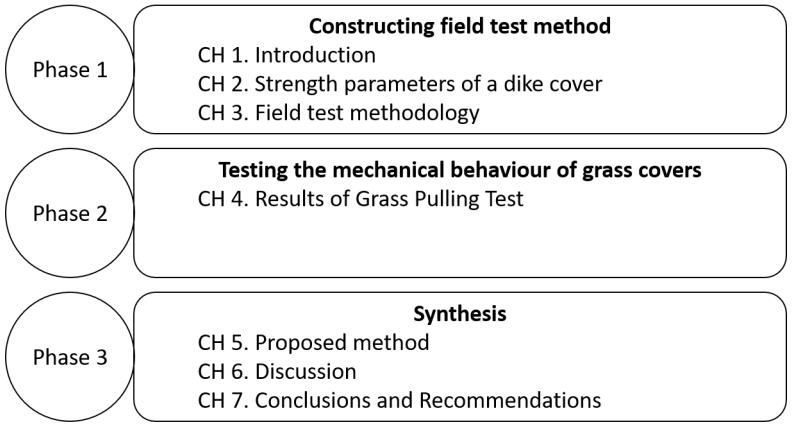

A large part of this thesis consists of field experiments, analysis and interpretation of the results of the field experiments. Based on a literature review, physical processes that possibly influence the mechanical behaviour of grass covers under tensile loads are identified in Chapter 2. Field experiments to examine the influence of the suggested process were designed and executed. The field experiments are described in Chapter 3. In Chapter 4, the results of the field experiments are presented. The results of these field experiments provided a better understanding of the processes that influence the mechanical behaviour of the grass cover and revealed new insights in the development of the process of damage accumulation. In Chapter 5, a method is presented that allows for an assessment of the grass cover resistance against repetitive loads. Finally, Chapter 6 and 7 provide the discussion, conclusions and recommendations of this thesis.

2

Strength Parameters of a Dike Cover

This section gives a description of the characteristics of grass covers on dikes. These characteristics are used to identify processes that possibly influence the mechanical behaviour of the grass cover. Starting with a introduction of grass cover composition on dikes. Furthermore, prevailing knowledge about grass cover strength, soil mechanics, soil strength and fatigue are elaborated upon. This chapter concludes with a summary of this literature review.

2.1. Composition of grass cover layer

Grass covers possess erosion resistant qualities. This attribute is mostly gained from the interaction between the soil and the root system (Muijs, 1999). The grass cover includes grassland vegetation rooted in a clay layer. Figure 2.1 gives a overview of the typical structure of a grass cover on a dike.

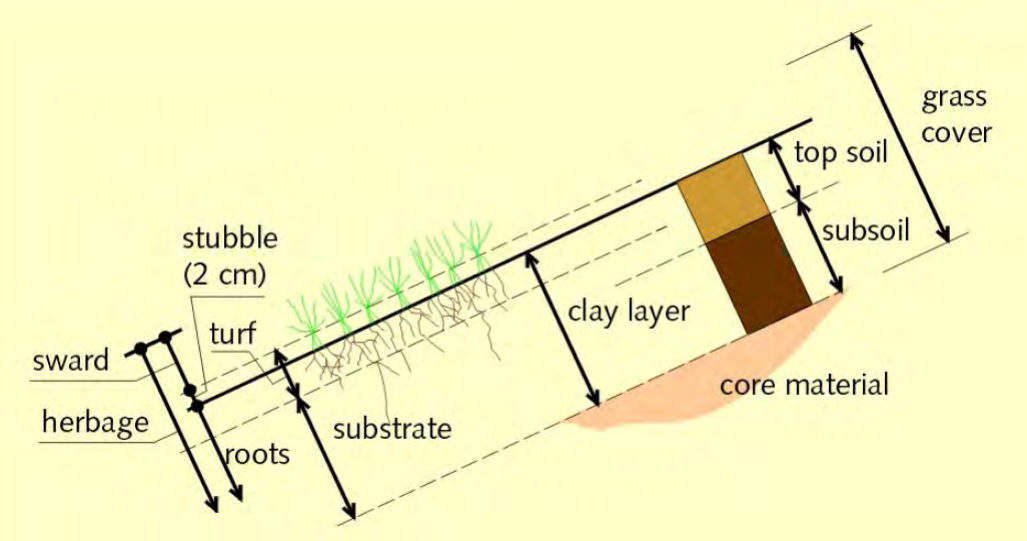

Figure 2.1: Structure and division of a grass cover Source : (Muijs, 1999)

The visible part of the grass cover consists of a flexible part, sward and a lower and is stiffer part the stubble. The subsurface zone with close packed roots and the stubble together form the turf. The porous turf layer consist of organic matter and sandy clay with a high root density and is elastic in moist conditions. The shrinking and expanding of soil in the unsaturated zone and biological activities cause the formation of cracks in the clay layer. Cracking formation produces a soil that consists of aggregates of various dimensions. Furthermore, roots secrete a sticky substance that glues soil particles together and cause cementation of the aggregates. The dimension of the clay aggregates increases with an increase in depth. The root structure of the grass connects the small clayey aggregates and prevents them from being washed out. The composition of aggregates and roots is called soil structure. The formation of the soil structure is a dynamic process. New aggregates are continuously formed and

demolished. Figure 2.2 gives a overview of the soil structure in clayey dikes.

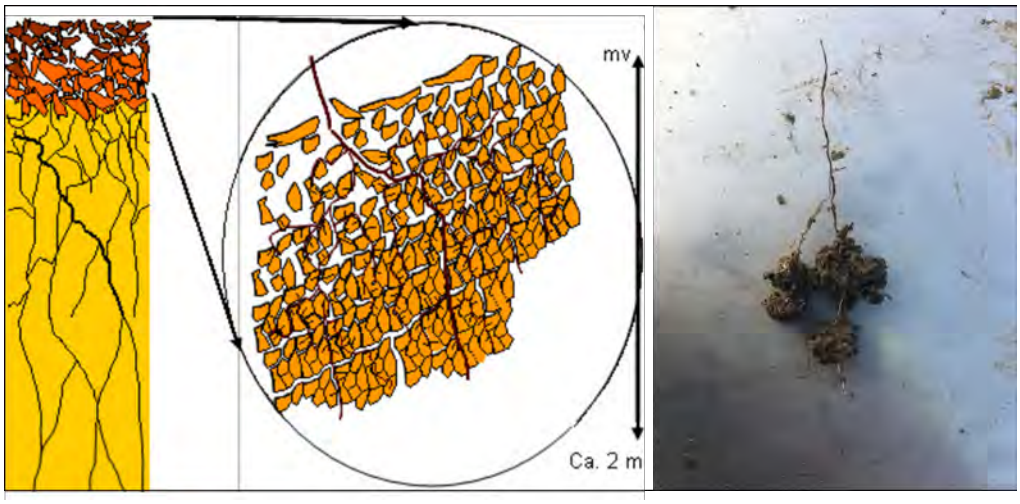

Figure 2.2: (a) Soil structure in clay layer. Source : (Van Ooijen, 1996) (b) Clay aggregates connected by roots. Source : Own picture November 2018.

The root structure of the vegetation can be divided into three parts (Van der Meer et al., 2015).

1. Layer with a high root density and small aggregates, also referred to as grass sod or top layer. This layer starts at the subsurface and continues to a depth of circa 5 cm. The grass sod characterised by elastic behaviour under moist conditions. under moist conditions
2. Layer with a root density of $3 - 10$ roots/dm^2.This Layer continues to a depth varying between $20 - 40$ cm.
3. Layer with a low root density, but still visible. Root density of $0.5 - 2$ roots/dm^2. The size of the aggregates is increased up to several dm. This layer is stiffer or plastic and less permeable compared to the two layers above.

As mentioned before, the strength of the dike cover depends on both the properties of the clay and the grass cover together. The grass strength near the surface is mainly determined by the root reinforcement, while in the deeper clay layer the strength is dominated by characteristics of the soil strength. The grass sod behaves elastic under moist conditions, where the deeper clay layer is stiffer and less permeable. Due to crack formation and the presence of a root system, grass covers show a higher hydraulic conductivity than bare clay. Typical values of hydraulic conductivity for grass covers vary between 10^{-5} to 10^{-4} m/s (Muijs, 1999).

2.2. Grass cover

Hoffmans et al.(2009) shows that the strength of the grass cover is determined by a combination of geomechanical strength of the clay within the grass sod and the strength of the grass roots. Also in other applications is shown that inclusion of fibre can improve the soil tensile strength. Li et al.(2014) showed that the mechanical interactions between fibre surface and soil particles are capable of sharing some tensile load and therefore increase the tensile strength of a soil body. An increase in fibre content results in an increase of the tensile strength.

During loading of a root reinforced soil, the root characteristics influence the deformation characteristics of the soil body. During failure, some roots break, and some roots are pulled out of the soil intact. The proportions of roots that break or pull out are determined by a combination of root characteristics, soil moisture and soil shear strength(Pollen, 2007).

The strength of the soil structure in a grass cover in terms of shear stresses as well as normal stresses can be described by the Mohr Coulomb criterion (Hoffmans et al., 2009). This representation is referred to as the Root model. Typically, the strength of roots is modelled by including the root cohesion (c_r) in the Mohr Coulomb criterion as shown in Equation 2.1(Hoffmans et al., 2009)

$$\tau_s = c_e \cos\phi_e + c_r + (\sigma - p_w)\sin\phi_e \tag{2.1}$$

Where τ_s is the soil shear stress, c_e is the effective soil cohesion, σ is the soil normal stress, ϕ_e is the effective internal friction angle and c_r is the influence of the strength of the roots modelled by the root cohesion. p_w is the pore water pressure, in saturated conditions usually positive. However above the water table the pore water pressure in clay can be negative. This negative pore water pressure has a positive influence on the cohesion of the sod. The suction pressure in the clay cover of a dike is usually less than $10kN/m^2$.

The root cohesion c_r can be theoretically determined based on the root tensile stress (σ_{root}), the root diameter (d_{root}) and the angle of shear deformation (ϕ). The determination of the root cohesion is depicted in Figure 2.3 and formulated in Equation 2.2 (Hoffmans et al., 2009).

$$c_r = \frac{A_{root}}{1m^2}(\sigma_{root,v}\tan\phi + \sigma_{root,h}) \tag{2.2}$$

The effect of the reinforcement of the grass cover by roots can also determined with field measurements. Tensile strength found with the Grass pull device as described by (Bijlard et al., 2017) appears to be higher than the theoretically determined tensile strength (Pijpers, 2013).

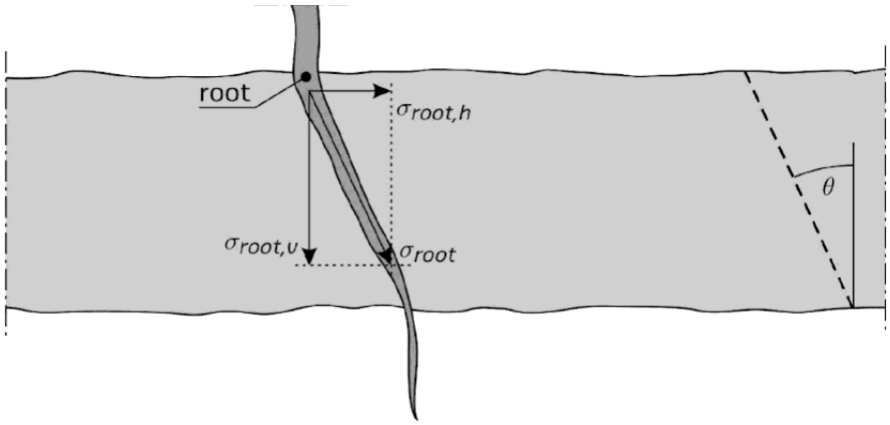

Figure 2.3: Root permeated into the soil. Source :Hoffmans(2012).

Based on the theoretical determination of the root cohesion is concluded that the number of roots is strongly correlated with strength of the grass cover. The root volume decays with an increase in depth under the soil surface. The decay of root volume is expressed by an exponential function related to depth (Sprangers, 1999; Stanczak and Oumeraci, 2012).

2.3. Soil mechanics

This section describes soil characteristics that provide resistance to a load. The stability of soil is largely dependent on the soil stresses within the soil body. During loading of a soil element, stresses are transmitted to the soil matrix. The presence of a liquid in this grain skeleton affects the stresses at the contact points between the grains. For a fully saturated soil, the stresses in the particles are determined by the contact forces between the grains and the water pressure around the grains. This principle is introduced in the concept of effective stress in saturated slopes (Terzaghi and Peck, 1948). This principle, also known as Terzaghi's effective stress principle states that the effective stress $\sigma^{'}$ is defined as a difference between the total stress σ and pore water pressure p (Verruijt, 2007).

$$\sigma = \sigma^{'} + p \tag{2.3}$$

The effective stresses govern the deformations in the grain skeleton. The relation between stresses and deformation are described by the Elasticity or Young's modulus (E) and the Shear modulus G. The definition of the moduli are described in Equation 2.4 and 2.5 (Winterwerp and Van Kesteren, 2004).

$$E = \frac{\Delta\sigma}{\Delta\varepsilon} \tag{2.4}$$

$$G = \frac{\Delta\sigma}{\Delta\gamma} \tag{2.5}$$

Denoted the stress increment by $\Delta\sigma$ and$\Delta\tau$, and ε and γ denote volumetric strain and deviatoric strain respectively. A visual representation of equation Equation 2.4 and Equation 2.5 is given in Figure Figure 2.4. In general, the relative deformation of the granular skeleton differs from the large scale deformation. Soil not only behaves linear elastic. The total strain is decomposed in an elastic part and a plastic part. The latter is irreversible. The relation between stresses and deformation is fully described by the $Stress - Strain$ relation found during tests.

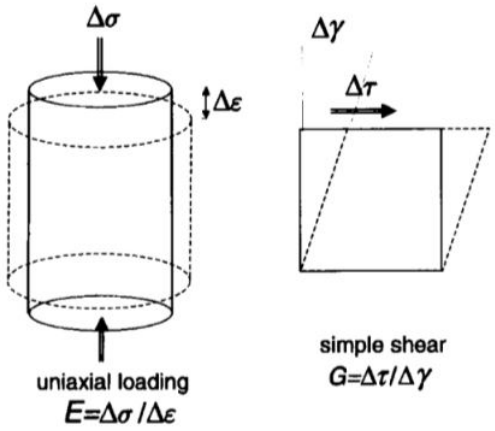

Figure 2.4: Elastic moduli. Reprinted from Winterwerp and Van Kesteren (2004).

Deformation of a soil, due to a change in effective stresses, results in a change in porosity. Therefore requires a inflow or outflow of the pore water. However, in a soil with a low permeability, this process may take a certain time. Resulting in a time dependent deformation. In drained conditions, the soil behaviour is determined by a combination of elastic behaviour and dissipation of pore water pressure (Winterwerp and Van Kesteren, 2004). This behaviour can be described by mechanics of porous media. The simultaneous deformation of the porous material and flow of pore fluid is the subject of the theory of consolidation. Considering the conservation of mass of the water and solid particles and the equilibrium equations of stresses acting upon a soil element, the behaviour of the soil element can be described (Verruijt, 2010). The process is simplified by a Kelvin-Voigt diagram with a spring element, representing elasticity, and a dashpot element representing effect of the pore water pressure development (Cuomo et al., 2011). During loading by overtopping waves, the grass cover has been assumed fully saturated. Also the loading rate has been assumed to be relatively high in relation to the time scale of the hydraulic conductivity of grasscovers in general. This might indicate that wave overtopping result in undrained behaviour of the soil. This effect is also supported by the results of Van Langevelde (2017).

2.4. Soil strength

The tensile failure of the cohesive sediments, such as clay, is mainly governed by the development of cracks in the soil (Tollenaar et al., 2017). Tensile failure starts with the opening of micro-cracks (Hallett and Newson, 2005; Winterwerp and Van Kesteren, 2004). Micro-cracks are often present in soil and form discontinuities in the skeleton, for example at the interface of large particles. By loading the soil element, stress concentrations at the edges of the micro-cracks occur. The micro-cracks grow and coalescence with other cracks. This result in formation of macro-cracks. The growth of micro-cracks can start before the bulk yield stress is reached (Winterwerp and Van Kesteren, 2004).

Hallett and Newson (2005) showed that the tensile failure of clay can be described as an elastic plastic process. They describe the fracturing of soil as a thermodynamic equilibrium process. This means that fracture occurs when imposed mechanical energy equals the energy required for fracture. During fracture propagation different stages can be distinguished. The first stage is the elastic stage of the material. Removal of the stress will cause the soil to return to its original state. This part of the fracture progression is characterised by the linear relationship between the applied force and the deformation. After passing the yield point, the deformation is plastic, which indicates the crack opening stage. During this phase, the increase in force applied produces sufficient energy build up to break the inter-particle bonds, leading to the generation of a fracture. The energy to generate a fracture is irrecoverable, this results in an irrecoverable deformation of the soil element. Once the fracture opens up, there is a

marked drop in stresses and crack propagation is started. According to Hallett and Newson (2005), a tangent modulus is parallel to the elastic region off fracture provides a reasonable estimate of Young's modulus. Its intersection with the applied force is approximately the yield point of the material (Hallett and Newson, 2005). Tollenaar et al. (2017) observed a drop in force necessary to continue the deformation at the yield point. The force decreases until the fracture reaches the stable ductile crack growth stage under an almost constant force. A graphic representation of the elastic plastic fracture mechanics is shown Figure 2.5.

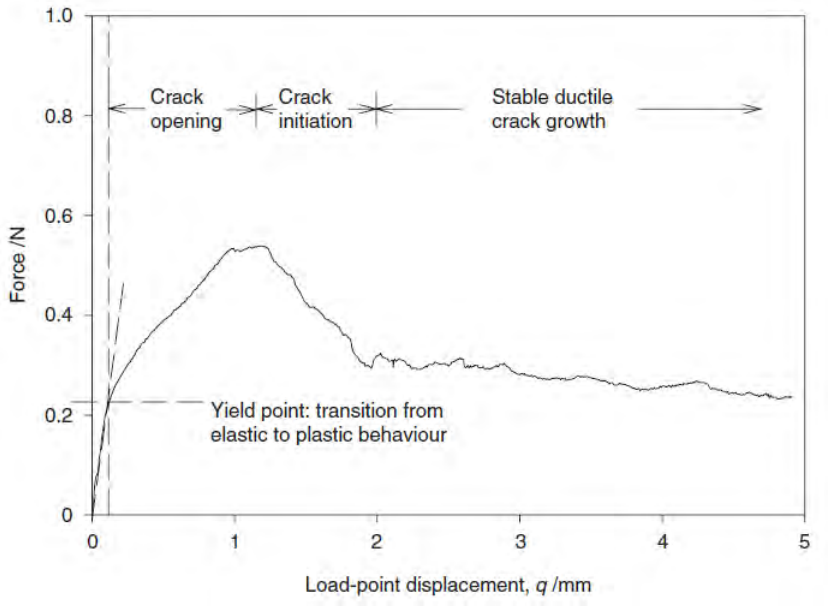

Figure 2.5: Force - Displacement diagram with the stages of crack growth in wet soil. Reprinted from Hallett and Newson (2005).

Winterwerp and Van Kesteren (2004) showed that loading of saturated soil with a tensile stress initially generates a pressure drop in de crack. As shown in Figure 2.5, the crack opens after the yield point. During the elastic and plastic stages the deformation of the soil induces suction. As a result of the suction no stress concentrations around the edges of the crack are generated. By continuous increasing of the applied force, the suction continues to build up until cavitation is reached. During the crack opening stage, the increase in suction and the decrease in soil surface are still able to provide resistance to the tensile force. The maximum tensile strength of the soil is reached when the suction leads to cavitation and soil particle separation lead to continuous crack growth (Hallett and Newson, 2005).

At relative large time scales, the matric suction due to loading with a tensile stress, results in pore water flow towards the crack. The suction decreases and, subsequently, stress concentrations at the edge of the crack appear. The drainage of cracks is governed by the consolidation coefficient of the sediment and the size of the crack (Winterwerp and Van Kesteren, 2004). For a constant tensile loading, the matric suctions starts with a equal stress as the tensile stress, at large times the matric suction dissipates due to local drainage of the crack and loading of the soil matrix.

2.5. Fatigue

During storm conditions multiple waves overtop the crest of the dike. It is likely that the dike does not fail after one wave, but reduces in strength per overtopping wave (Bijlard, 2015). It seems plausible that fracturing of the clay occurs and subsequently the roots are loaded. During one loading cycle some roots break, but quite some others only get partly pulled out or deform. This way the force is redistributed to other roots so the soil keeps some strength. This could be seen as fatigue of the grass cover. The results of a fatigue test executed by Hoffmans (Pijpers, 2013; Steendam et al., 2014) are depicted in Figure 2.6.

Description of the influence of fatigue of the grass sod might be useful to predict the effect of the cyclic nature of wave overtopping during storm conditions. To the knowledge of the author, the influence of fatigue has only been described in literature on a very limited scale. However, the results of Hoffmans (Pijpers, 2013; Steendam et al., 2014) and Bijlard (2015) indicate that fatigue might influence the

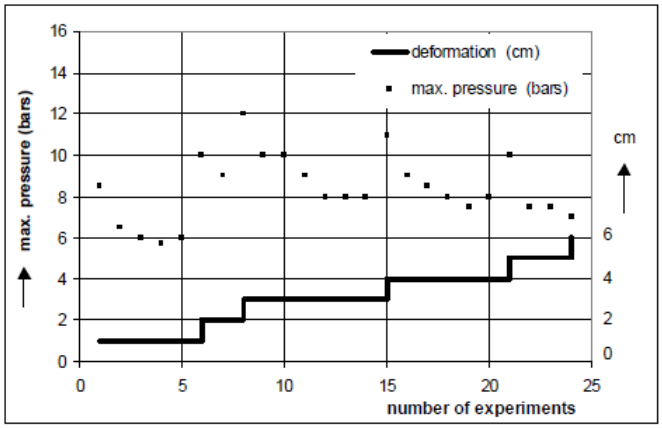

Figure 2.6: Fatigue of the grass cover. The effect of fatigue is shown by imposing a constantly increasing displacement. Every imposed displacement is repeated several times, after which the displacement is increased. A clear reduction of the required pull force can be seen. Source: Pijpers(2013).

strength of the grass sod. Moreover, the cumulative overload method developed by Van der Meer et al. (2010), suggest that the grass cover features some kind of fatigue limit. The cumulative overload method is described in more detail in Appendix A.

Tensile failure of clay is mainly governed by fracture development (Hallett and Newson, 2005; Tollenaar et al., 2017; Winterwerp and Van Kesteren, 2004). This process shows similarities with the tensile failure of other materials which are also governed by fracturing, e.g. concrete and asphalt (Cornelissen, 1984; Li, 2013; Yang and Den Uijl, 2019). According to Cornelissen (1984), fracturing of concrete due to tensile loading is influenced by repeated loading, so fatigue plays a part in the strength of the material. Development of the fracture process due to repeated loading is similar to the description in Section 2.4. Starting with stress concentration around discontinuities or micro-cracks. When stress concentrations are high enough, the crack starts to grow during subsequent load cycles. Final failure occurs when the reduced cross-section becomes insufficient to carry the peak load, even though the gross stress is much less than would normally cause yield or failure in a tensile specimen.

Fracturing can be described as an energy-balance process (Hallett and Newson, 2005; Roylance, 2001b; Yang and Den Uijl, 2019). This process results in elastic plastic nature of fracturing and has large influence on the effect of a cyclic load. Loading by forces with sufficient energy result in energy dissipation due to generation of a fracture. The residual strain is accumulated and result in an increasing initial strain for every loading cycle. The effect of crack formation on the strain of the material is show in Figure 2.7.

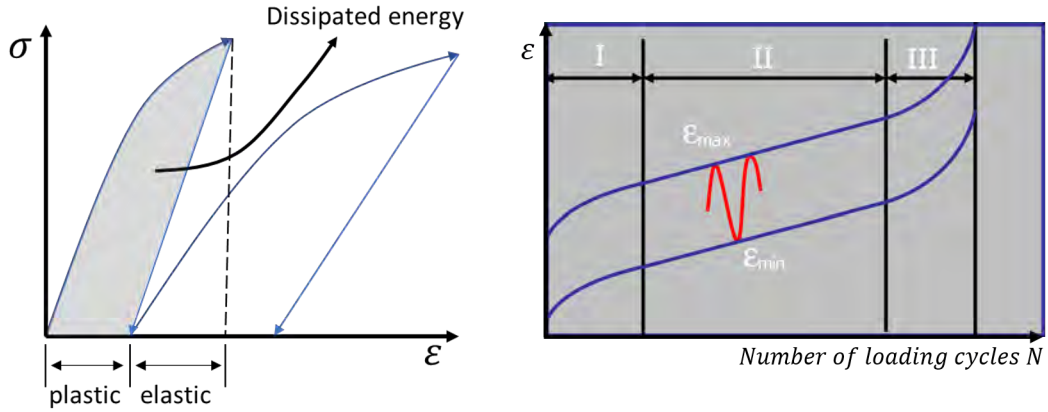

Figure 2.7: Plastic deformation is irrecoverable and is accumulated during successive loading cycles. The left panel shows typical plastic and elastic behaviour as found for concrete under cyclic loading. The right panel show the strain (ε) development during cyclic loading of a specimen. Adapted from Yang and Den Uijl (2019).

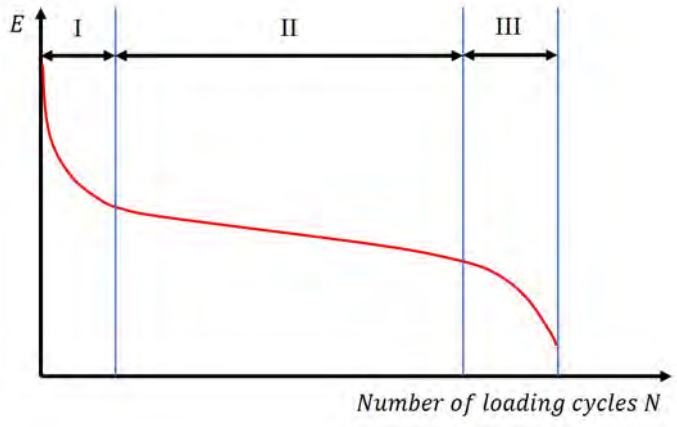

Figure 2.8: The successive phases of stiffness decrease due to fatigue. Reprinted from Li (2013).

Based on the development of the stiffness and strain of a specimen, the fatigue process has been divided in three distinguished phases(Li, 2013; Yang and Den Uijl, 2019), as indicated by Roman numerals in Figure 2.7 and Figure 2.8. It is important to bear in mind that Figure 2.7 and Figure 2.8 show the fatigue process for a cyclic load which is fluctuating at constant stress amplitude.

I. Initial crack formation.
   During this phase, the stiffness of the test specimen decreases rapidly due to the development of microcracks by the repetitive loading.

II. Stable crack growth.
   Microcracks grow at a stable rate resulting in a slow decrease of the stiffness of the specimen.

III. Unstable crack growth.
   Different microcracks coalesce, resulting in one or a few dominating cracks. Macrocracks start to develop and failure occurs at the end of this phase.

In general, fatigue cracks spend most of their life as very small cracks in the initial crack formation and the stable crack growth phase. During this phase, the inclination of the $\varepsilon - N$ curve or the $E - N$ is relatively stable. The same applies for the stiffness of the specimen. Therefore the gradient of these curves is found to be a good measure to predict the fatigue life, in number of cycles to failure. For example Cornelissen (1984) showed this for concrete.

The most important concept is the $S - N$ diagram. To construct a $S - N$ diagram a constant cyclic stress amplitude is applied to a specimen. The number of loading cycles until the specimen fails is determined. This process is repeated for different stress amplitudes until a full $S - N$ curve is determined. An example of a $S - N$ curve is depicted in Figure 2.9.

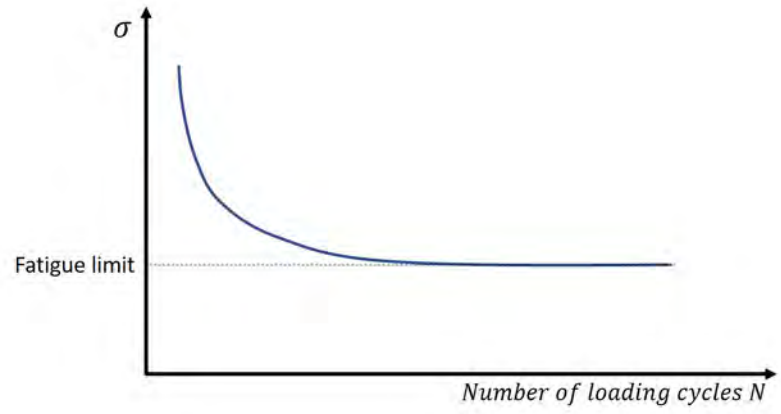

Figure 2.9: S-N curve depict the number of loading cycles until a specimen fails for different stress amplitudes. Adapted from Yang and Den Uijl (2019).

In general, variability in cycles at a given stress is quite large. Resulting in a large amount test is required to define a $S - N$ curve with statistical confidence. Obtaining a full $S - N$ curve is therefore

a tedious and expensive procedure. In some materials, the curve flattens out eventually, so that below a certain endurance limit failure does not occur for an unlimited number of cycles, also referred to as the fatigue limit. Below this stress level only elastic deformation occurs, and no damage is caused to the material. This makes the fatigue limit of a material a desirable design load. The fatigue limit is generally denoted by S_0.

When the cyclic load level varies during the fatigue process, a cumulative damage model is often utilized (Roylance, 2001a). The Load spectrum is simplified into load ranges. The damage done by each range in the spectrum is defined as $\frac{n}{N}$. Here n is the number of load cycles in the range and N is the number of loading cycles until the specimen fails if only that specific load range was applied. In some materials, other characteristics describe the cumulative damage more effectively. For instance, the strain rate (Cornelissen, 1984) or the stiffness of the material (Yang and Den Uijl, 2019).

2.6. Summary

The literature review provided valuable insight into the physical processes and variables that might influence the erosion resistance of grass covers against pull-out erosion. Based on this literature review, the following findings were reported:

1. Tensile behaviour of cohesive sediments.
   The tensile strength of the cohesive sediments, such as clay, is mainly governed by the development of cracks in the soil. This process is largely influenced by the development and dissipation of suction in the soil element. The development and dissipation of suction in the soil element is determined by the hydraulic conductivity of the grass cover. The failure process due to cracking can be described as an elastic plastic process. The transition between the elastic and plastic range is indicated by the yield point.
2. Tensile behaviour of grass roots.
   The tensile strength of grass roots is determined by the slip and breakpoint of the roots. These characteristics are determined by a combination of root properties, soil moisture and soil shear strength.
3. Fatigue of the grass cover.
   Previous research suggest that grass covers are subject to fatigue. Deformation of the grass cover might behave as an elastic plastic process and therefore feature some kind of a fatigue limit. Loading below this stress level causes no damage to the material, this makes the fatigue limit a desired design load.

Since the erosion resistance of grass covers against pull-out erosion is assumed to be determined by a combination of geomechanical strength of the clay within the grass sod and the strength of the grass roots, it is suggested that physical processes described in finding one and two apply to the erosion resistance of grass covers against pull-out erosion. The findings concerning the physical processes and variables that might influence the erosion resistance of grass covers against pull-out erosion were investigated in this study.

3

Field Test Methodology

Literature suggests that the erosion resistance of grass covers against pull-out erosion is influenced by the physical processes and variables as summarized in Section 2.6. The influences of these processes were tested in order to gain insights into the mechanical behaviour of grass covers. This section starts with a description of the method used to preform these tests. Second, a description of the tested variables is given and third, the applied method to analyse the test results is described.

3.1. Methodology of grass pull test

The test set-up of the sod pulling test consists of a small pull frame with dimensions of $20 \times 20cm^2$, see Figure 3.1 (a), and a pulling mechanism consisting of a hydraulic cylinder and a manually operated hydraulic pump, see Figure 3.2. In order to anchor the pull frame, the grass sod was cut loose at two opposite facing sides and was excavated at both sides up to 8 cm depth as shown in Figure 3.1(b). Five pins are inserted below the surface of the grass through the soil in order to anchor the pull frame to the grass sod sample. An anchored pull frame is shown in Figure 3.1(c).

(a) Pull frame. (b) Grass sod cut loose to enable installation of the pull frame. (c) Anchored pull frame.

Figure 3.1: The test set-up of the sod pulling test, pull frame.

After anchoring the pull frame to the sod, the pulling mechanism consisting of a cylinder and a supporting frame is placed. The pulling mechanism is placed directly above and connected trough a hinge to the pull frame as depicted in Figure 3.2. Once the cylinder is connected to the pull frame, the device can impose a tensile force on the grass sod. The pull frame is connected to the cylinder through a HBM U2A load cell, to measure the imposed force. Vertical displacement is measured using an ASM WS1 draw-wire displacement sensor. The installation and calibration of sensors is done by Deltares.

Figure 3.2: The test set-up of the sod pulling test, pulling mechanism.

3.1.1. Measurements

For each test the following characteristics are measured:

- Force as function of time.
  The force was measured at a sample rate of $100\ Hz$, utilizing a HBM U2A load cell. The measured force was corrected for the weight of the anchor frame and pins.
- Displacement as function of time.
  The displacement was measured at a sample rate of $100\ Hz$, utilizing an ASM WS1 draw-wire displacement sensor.
- Weigth of pulled sod.
- Width of pulled sod.
- Height of pulled sod (average of three measurements combined with estimated percentage of occurrence).
- Length of roots (average of three measurements combined with estimated percentage of occurrence).

More details about the method to determine the dimensions of the tested grass cover sample are described in Section 3.3.

3.2. Variables

To support the understanding of the erosion resistance of grass covers against pull-out erosion, the influence of the in Section 2.6 suggested physical processes and characteristics were tested. Based on physical processes and characteristics, the following variables are determined: load regime, degree of saturation and location. The variables are elaborated into more detail in the following section. Figure 3.3 gives a summary of the determination of the test variables.

Constructing field test method

Physical processes and characteristics :	Tested variables:
1. Influence of tensile behaviour of cohesive sediments.	
• The development and drainage of matric suction in the soil element.	→ Loading Regime + Degree of saturation + Location
2. Influence of tensile behaviour of grass roots.	
• Root properties	→ Location
• Soil shear strength	→ Location
• Soil moisture	→ Degree of saturation
3. Fatigue of the grass cover.	
• Damage accumulation.	→ Loading Regime
• Clear transition between the elastic and plastic range.	→ Loading Regime

Figure 3.3: Test variables based on findings of literature review as described in section 2.6.

3.2.1. Load regime

A stepwise increased cyclic load, a stepwise increased constant load and maximum force load regime were performed during the field tests. The purpose of these three load regimes were to determine the possible effect of damage accumulation due to loading of the grass cover, the possible effect of development and drainage of matric suction in the grass sod element during loading, and the presence of a clear transition between the elastic and plastic range respectively.

Stepwise increased constant load

To study the possible effect of development and drainage of matric suction in the grass sod element during loading, a stepwise increased constant force - controlled lifting load for two different degrees of saturation was tested. In Figure 3.4 an indication of the induced load is given.

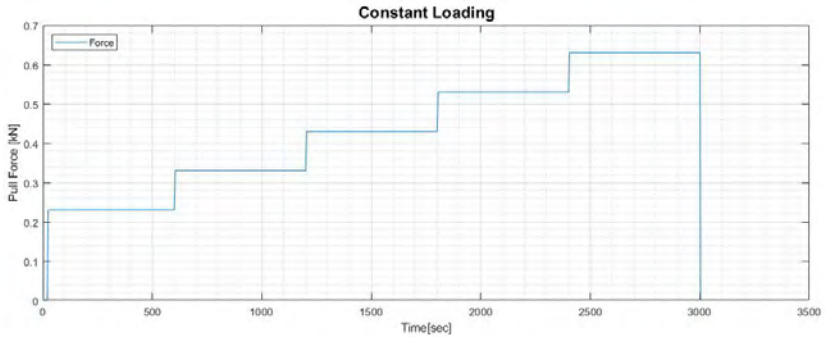

Figure 3.4: Variable: Load Regime. During constant loading, the grass sod is loaded with a constant load. The load increases every 10 minutes with circa $0.1kN$, starting with a load of circa $0.2kN$. This process proceeds until failure occurs.

During this test damage accumulation due to a constant load is tested as well. Before testing, there was no indication if loading with low stresses would induce failure. To prevent extremely time consuming tests, it was decided to stepwise increase the constant load. Furthermore, this approach might reveal a kind of fatigue limit of the grass cover.

Stepwise increased cyclic load

To determine the effect of damage accumulation due to the repetitive loading, the grass sod is cyclically loaded by a force - controlled lifting load. The construction of a complete $S - N$ curve provides most insight into damage accumulation. However, construction of a complete $S - N$ curve is not feasible. Therefore, the load as depicted in Figure 3.5 was designed.

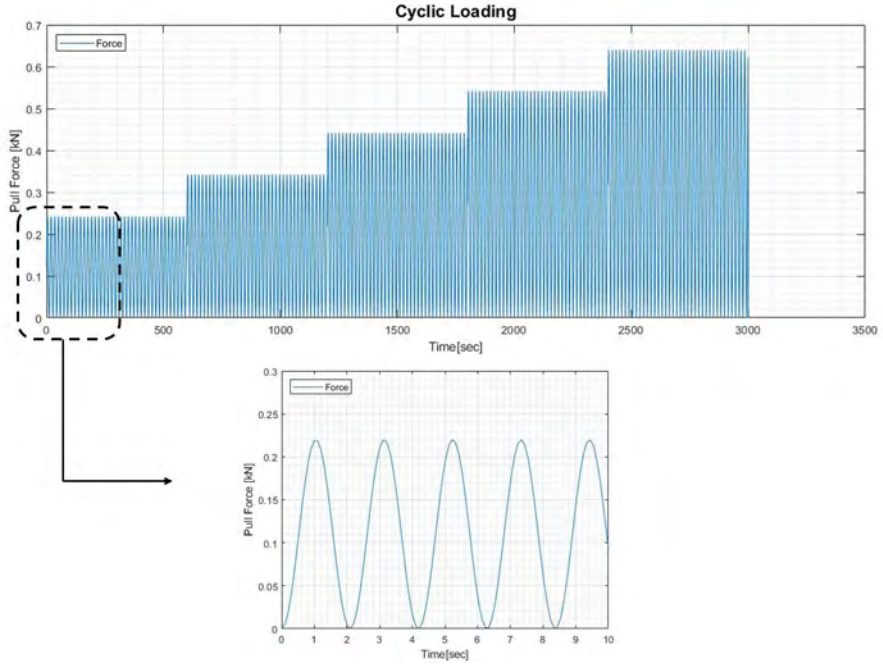

Figure 3.5: Variable: Load Regime. During a stepwise increased cyclic load, the grass sod is repetitively loaded with a relative constant amplitude, mean load and period. The amplitude of the load increases every 10 minutes with circa $0.2kN$, starting with a load of circa $0.2kN$. This process proceeds until failure occurs.

The amplitude of the cyclic load is stepwise increased for multiple reasons. 1.) To prevent extremely time consuming tests. Before testing, there was no indication if loading with low stresses would induce failure of the grass cover or how many loads would lead to failure. 2.) The stepwise increase of the cyclic load might reveal a kind of fatigue limit of the grass cover.

Maximum force load
The load regime as described by Bijlard (2015; 2017) was tested as well. The maximum load was tested in combination with the other load regimes, in order to study the presence of a clear transition between the elastic and plastic behaviour of the grass sod by means of a yield point as described in Section 2.4.

In addition to insights into the physical processes, this approach provides insight into the possibilities to determine a strength metric with a simple and a relative time efficient method as well. Under this load regime the grass sample is pulled out at once, by a displacement - controlled lifting load. Herewith the Force - Displacement relation up to the maximum tensile strength is determined.

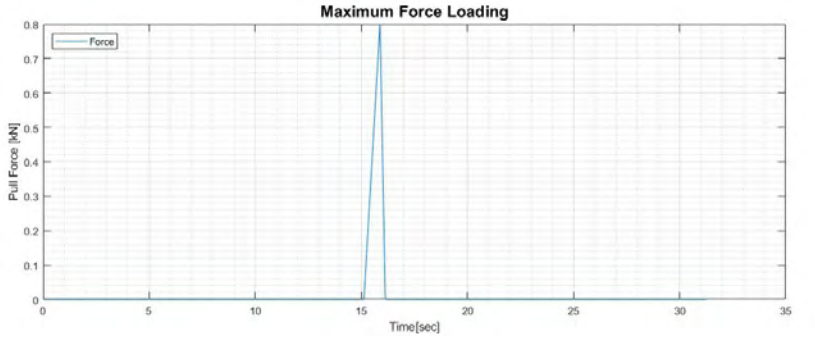

Figure 3.6: Variable: Load Regime. During maximum force loading, the grass sod is loaded with a constant pull rate until failure occurs.

It should be noted that the Grass sod pull device has been manually operated. The depicted load regimes in Figure 3.5 to 3.6 are idealised representations of the induced load during the tests. Moreover, the steps in the load amplitude used during cyclic loading and the steps in load during constant loading, are chosen and based on practical considerations during the execution of the field tests and limitations of the test system.

3.2.2. Degree of saturation

During normal conditions, the grass cover is not completely saturated. However, during storms conditions (which can be expected during overtopping waves) the grass cover will become more and more saturated over time. In order to gain insight into the effect saturation of the grass cover, tests are performed during submerged and non-submerged conditions. Furthermore, the assumption is made that grass covers conduct air much easier than water. Therefore, this variable is used to investigate the possible occurrence of suction pressure as described in section 2.4.

Figure 3.7: Variable: Degree of saturation. Box used to perform grass pulling test in submerged conditions.

In order to execute grass tensile tests under submerged conditions, a box with dimensions of $40 \times 80 \times 20cm$ (Length x Width x Height) is used. The box in installed over the anchored pull frame and hammered partly into the soil. An example is given in Figure 3.7. The box is filled with water, at least 30 minutes before executing the test. Fresh water is used to prevent dying of the grass.

3.2.3. Locations

To gain a better understanding of the grass cover strength, field experiments have been conducted at the Wadden Sea dike near Oosterbierum and at the IJssel dike near Zwolle. The grass cover quality of both locations in terms of coverage is comparable. However, the grass covers differ in terms of soil composition. The Wadden Sea dike is characterised as clay with a low low sand content. The IJssel dike on the other hand is characterised by clay with a high sand content. Based on the difference in sand content of the clay, it can be assumed that the hydraulic conductivity of the clay at the IJssel dike is larger than the hydraulic conductivity of the clay at the Wadden Sea dike. However, this assumption is not tested. However, the assumption is supported by observations during the experiments. Drainage of the box, depicted in Figure 3.7, happened considerably faster at the IJssel dike.

3.2.4. Number of cuts

In order to install and anchor the pull frame to the grass cover, the grass cover sample is cut loose at two opposite facing sides. This procedure disturbs the strength of the grass cover. By also performing the tests with four sides of the grass sod cut loose, insights in the cohesion or shear strength of the grass sod are gained. Cutting of the sides takes place during the grass cover sample preparation. The location of the cuts is indicated in Figure 3.8.

(a) Two sides cut loose. (b) Four sides cut loose.

Figure 3.8: Variable: Number of cuts. Location of cuts.

(a) Two sides cut loose. (b) Four sides cut loose.

Figure 3.9: Variable: Number of cuts. Difference of failure plane between two and four cuts.

With four sides cut loose, the sides do not contribute to the measured strength during lifting of the sod, only the bottom of the sod resists against the uplifting force. Figure 3.9 shows that the contribution of the sides of the grass sample results in a different location of the failure plane. The location of the failure plane provides valuable insights into the strength of the grass cover.

3.3. Methodology to analyse the test results

The raw data of the tests, measurements of force, displacement and sod dimensions, are used to study the mechanical behaviour of the grass sod. In the following section the method to determine the influence of the in section 2.6 suggested physical processes and characteristics are described.

3.3.1. Influence of cohesive sediments on grass cover behaviour

The expected development and drainage of matric suction in the soil element due to volumetric strain result theoretically in a time dependency of the displacement that is only influenced by the hydraulic conductivity K_s of the grass sod. Based on a difference in conductivity of the grass sod for water and air, the occurrence of this process was tested by analysing the displacement rate under a stepwise increased constant load for submerged and non submerged conditions. The time to reach 80% of the final displacement was determined, Figure 3.10 shows an example.

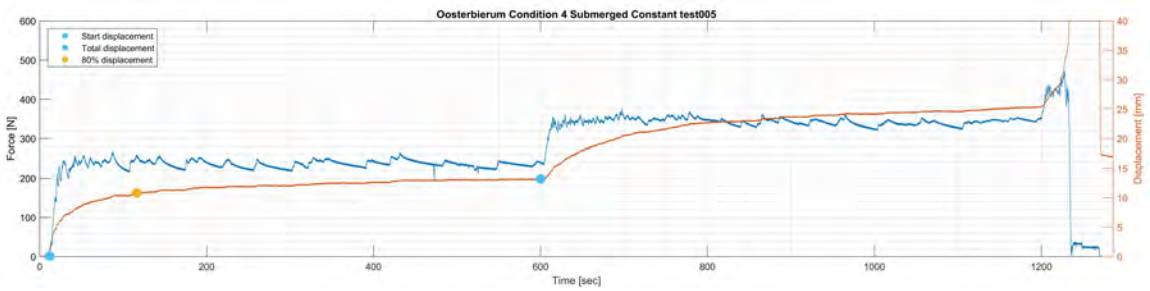

Figure 3.10: Displacement rate induced by a stepwise increased constant load. The blue dots indicate the total or final displacement as result of the induced load during the first 600 seconds of loading. The yellow dot indicates 80% of the final displacement.

The development of the elasticity of the grass cover over time is analysed based on the stress (σ) and strain (ε) as described in Equation 3.1

$$Elasticity = \frac{\sigma}{\varepsilon} \tag{3.1}$$

The elasticity modulus (E) is determined based on the final displacement due to the induced load after 600 seconds according to Equation 3.2.

$$E = \frac{\sigma}{\varepsilon_\infty} \tag{3.2}$$

Where stress (σ), strain (ε) and final strain (ε_∞) are determined based on the dimensions of the sod as measured after the sod was lifted out the grass cover and the measured force and displacement. The formulae to determine stress and strain are shown in Equation 3.3.

$$\begin{aligned} \sigma &= \frac{Force}{Width\,of\,pull\,frame \times Width\,of\,grass\,sod} \\ \varepsilon &= \frac{Displacement}{Mean\,height\,of\,pulled\,out\,sod} \\ \varepsilon_\infty &= \frac{Final\,displacement}{Mean\,height\,of\,pulled\,out\,sod} \end{aligned} \tag{3.3}$$

3.3.2. Influence of grass roots on grass cover behaviour

The behaviour of the grass roots under tensile load are assumed to differ for failure due to slipping or breaking of the roots. To determine the failure mode of the grass roots, no direct measurement proportions of roots that break or pull out were determined. The average length of the visible part of the grass roots, as described further on, was assumed as good an approximation. To use this measure, the root density was assumed to be constant at one test location.The depth where the failure plane develops is the depth where the tensile stress exceeds the tensile strength. Therefore, the dimensions of the lifted grass sod provides information of the total strength of the grass cover and the development of the failure plane. To determine the effect of the tested variables on the behaviour due to tensile strength of the grass roots, the dimensions of the specimen were measured. After lifting the grass sod out of the specimen the width, height and root lengths are determined.

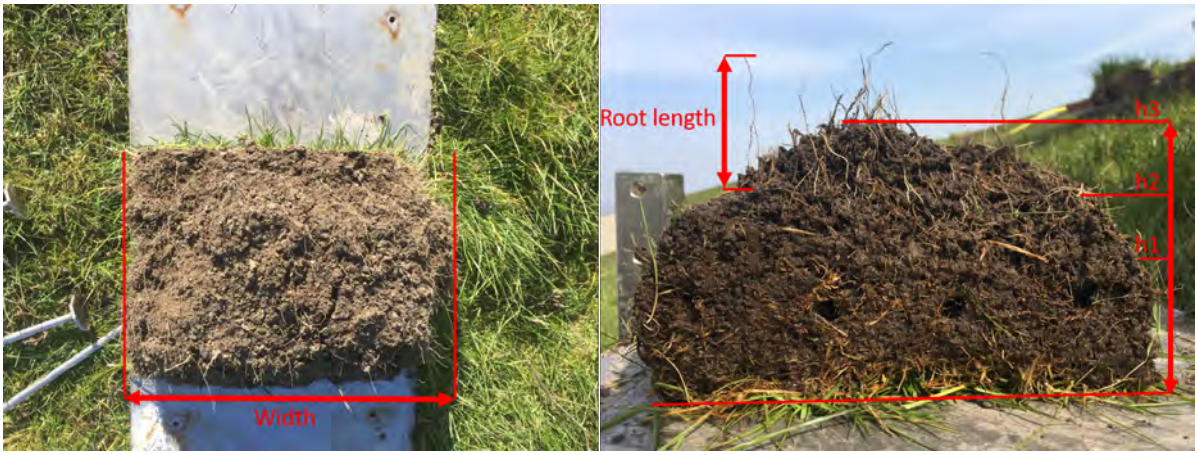

Figure 3.11: The measured dimensions are indicated by the red arrows.

Figure 3.11 shows the measured dimension. The length perpendicular to the width of the grass sod is $20cm$, since the cutting template and pull frame have dimensions of $20x20cm^2$. The width of specimen tested with four sides cut is $20cm$. The average sod height is estimated based on three heights with a large surface area in combination with the estimated percentage of occurrence. The three estimated heights are depicted with h1, h2 and h3 in Figure 3.11. For each of the three surface areas, the average root length is estimated. The root length is measured from the tip of the root to the grass sod as depicted in Figure 3.11.

3.3.3. Fatigue of the grass cover

To determine if damage accumulation occurs, the load to cause failure of the grass cover was determined. The failure point is defined as the point at which the grass cover is not able to resist the load as induced according to the load regimes, leading to substantial loss in mechanical properties, i.e. ongoing deformation and a drop in measured force.

Elastic - Plastic behaviour

To determine whether the grass cover deformation behaves elastic - plastic and whether a clear distinction exists between the elastic and plastic range of deformation, the grass cover behaviour under tensile loading was tested. The analysis of the behaviour of the grass cover is based on the measured displacement due to the induced force, the derived Stress - Strain relation and the development of elasticity of the grass sod. In some cases during tests with a stepwise increased cyclic load, initial stress and displacement at the beginning of a load cycle occurred. To account for this effect, a difference was made between the total elasticity according to Equation 3.2 and the partial elasticity according to Equation 3.6.

$$PartialElasticity = \frac{\Delta\sigma}{\Delta\varepsilon} \tag{3.4}$$

with:

$$\begin{aligned} \Delta\sigma &= \frac{\Delta Force}{Width\,of\,pull\,frame \times Width\,of\,grass\,sod} \\ \Delta\varepsilon &= \frac{\Delta Displacement}{Mean\,height\,of\,pulled\,out\,sod} \end{aligned} \tag{3.5}$$

$\Delta\sigma$ and $\Delta\varepsilon$ are based on the local maxima and minima of the induced force and the resulting displacement per load cycle as described in Equation 3.6.

$$\begin{aligned} \Delta Force &= local\,maximum\,Force - corresponding\,local\,minimum\,Force \\ \Delta Displacement &= local\,maximum\,Displacement - corresponding\,local\,minimum\,Displacement \end{aligned} \tag{3.6}$$

The local maxima and minima of the measurements of force and displacement are determined with standard functions based on spline intergation available in MATLAB R2019a. Figure 3.12 shows an example of this method.

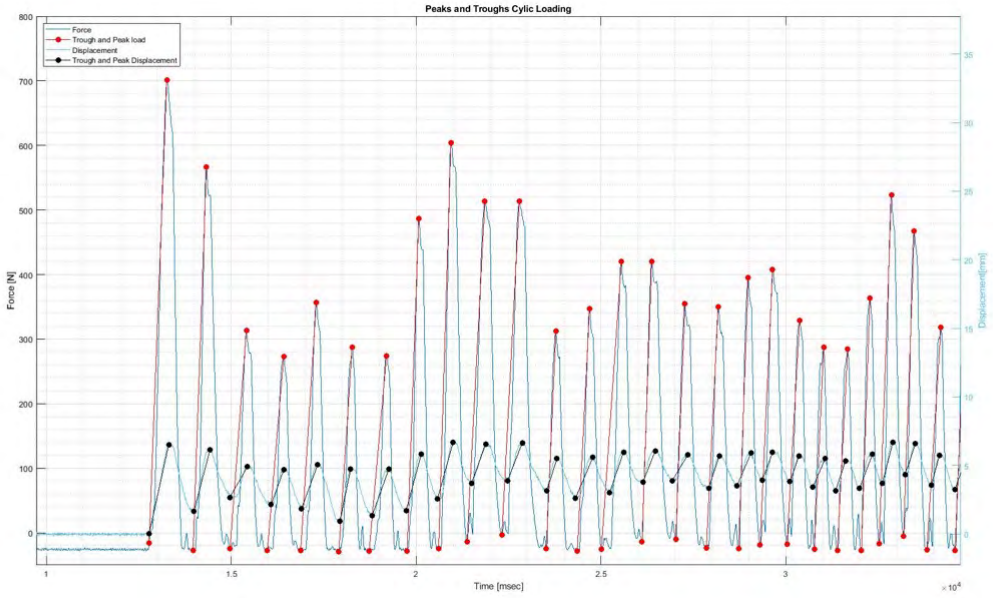

Figure 3.12: The local minima and maxima are determined with standard functions based on spline interpolation available in *MATLAB R2019a*.

3.3.4. Load metric for cyclic loading

The manual operation of the Grass sod pull device resulted in a deviation of the cyclic load regimes in comparison with the intended loading as described in Figure 3.5. To get a good indication of the applied load during testing, two load metrics have been determined for the executed tests. The mean load and the mean maximum load were determined for all tests. The latter is based on the results of the analysis of local maxima as described in Figure 3.12.

3.4. Execution of grass pulling tests

The videos in this section give an impression of the execution of grass pulling tests in the field.

Video of execution of maximum force test under non submerged conditions. Scan QR code to start video.

Execution of maximum force test under submerged conditions. Scan QR code to start video.

Execution of a cyclic load test under non submerged conditions. The video shows the last part of the test up to failure of the grass cover. Scan QR code to start video.

4

Results of Grass Pulling Test

In this chapter the results of the field tests are discussed. The field tests were executed between the 11th of March and the 25th of April 2019. An overview of the number of executed tests for each type as described in Chapter 3 is shown in Table 4.2 and Table 4.1. Note that the number of tests is determined by the available timespan for this research.

Table 4.1: Number of performed tests at the Waddensea dike near Oosterbierum

	Non Submerged		Submerged	
Load regime	2 sides cut	4 sides cut	2 sides cut	4 sides cut
Cyclic load	1	5	6	11
Stepwise increased constant load	6	5	7	6
Maximum Force	15	15	10	12

Table 4.2: Number of performed tests at the IJssel dike near Zwolle

	Non Submerged		Submerged	
Load regime	2 sides cut	4 sides cut	2 sides cut	4 sides cut
Cyclic load	0	1	5	4
Stepwise increased constant load	1	1	2	4
Maximum Force	21	2	2	5

The influence of 1.) Tensile behaviour of cohesive sediments, 2.) Tensile behaviour of grass roots, and 3.) Fatigue of the grass cover was tested. In the following sections, a summary of the results is presented. An complete overview of the test results is presented in Appendix C and D.

In the remainder of this chapter, boxplot diagrams are used to graphically depict the test results. On each box, the central mark indicates the median, and the bottom and top edges of the box indicate the 25th and 75th percentiles, respectively. The whiskers extend to the most extreme data points, and the outliers are plotted individually using the '+' symbol. The sample size is depicted together with the label of the considered variable.

Test execution problems
A manually operated grass sod pull device was used to execute the tests. This has resulted in a deviation of the induced loads with the intended loads during testing. During the stepwise increased constant load tests, this has led to fluctuations of the load of circa $50N$ around a constant value of $200\,N$. Figure 4.1 gives an indication of the deviation of the induced load. For the cyclic load tests the manual operation of the grass pull device has resulted in a deviation of the amplitude and frequency of the imposed load. The amplitudes deviate in some cases up to a factor two with the intended load. A frequency of $1-2Hz$ turned out to be most natural to impose. However, a large variation in frequency has occurred during testing. Especially inducing loads that resulted in high displacement caused large deviations from the intended load. The displacement - controlled maximum force loading were not executed under a constant displacement rate, as was intended. The maximum force loading tests were executed with a average displacement rate of circa $2\,cm/s$.

4.1. Influence of cohesive sediments on grass cover behaviour

The behaviour of the grass sod under stepwise increased constant load is characterised by an ongoing displacement whereby a decrease in elasticity is observed. The displacement rate and elasticity rate decreases within the timespan of 600 seconds until a more or less constant value of displacement and elasticity is reached. This constant value of the elasticity is assumed to be the elasticity modulus E of the grass cover. After an increase of the load, the grass cover samples showed similar behaviour as they did before the increase of the load. However, after an increase of the load a majority of the grass cover specimen did not reach a constant displacement level. An increase of the load also resulted in a decrease of elasticity. Ongoing displacement eventually causes failure of the grass cover. Depending on the strength of the specimen, failure occurred at different load levels. Figure 4.1 illustrates typical behaviour under stepwise increased constant load.

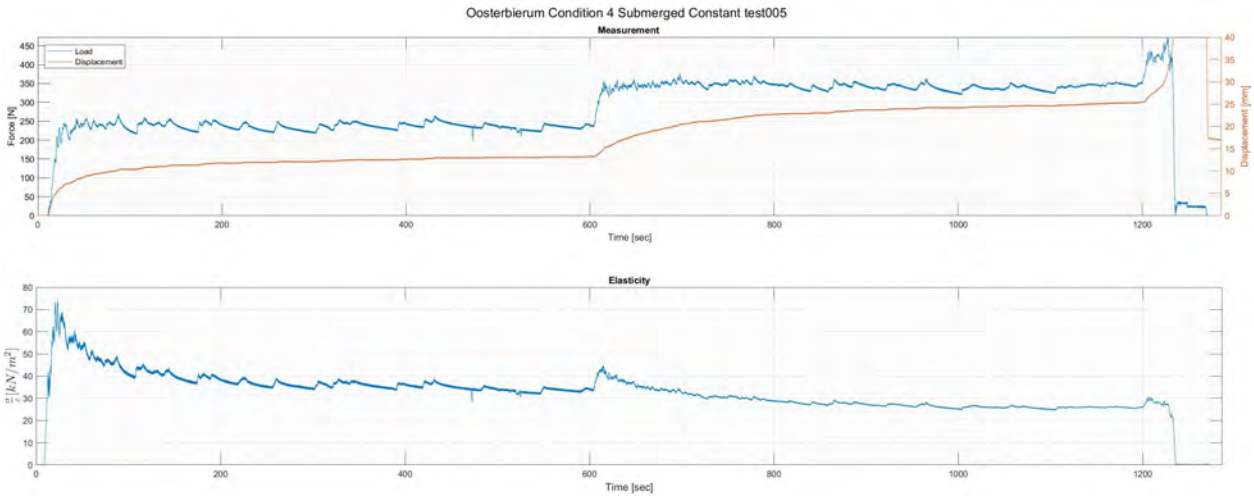

Figure 4.1: An example of typical development deformation and elasticity of the grass cover due to stepwise increased constant load. In the top panel the raw measurement of load and displacement is depicts. The lower panel depicted the resulting elasticity of the grass cover.

The development and dissipation of matric suction in the grass sod was tested by analysing the displacement rate under stepwise increased constant load for submerged and non submerged conditions. The time needed to reach 80% of the final displacement between submerged and non submerged conditions for two locations under stepwise increased constant load was compared. This method is described in Section 3.3. Figure 4.2 shows the results of the analysis of the displacement rate.

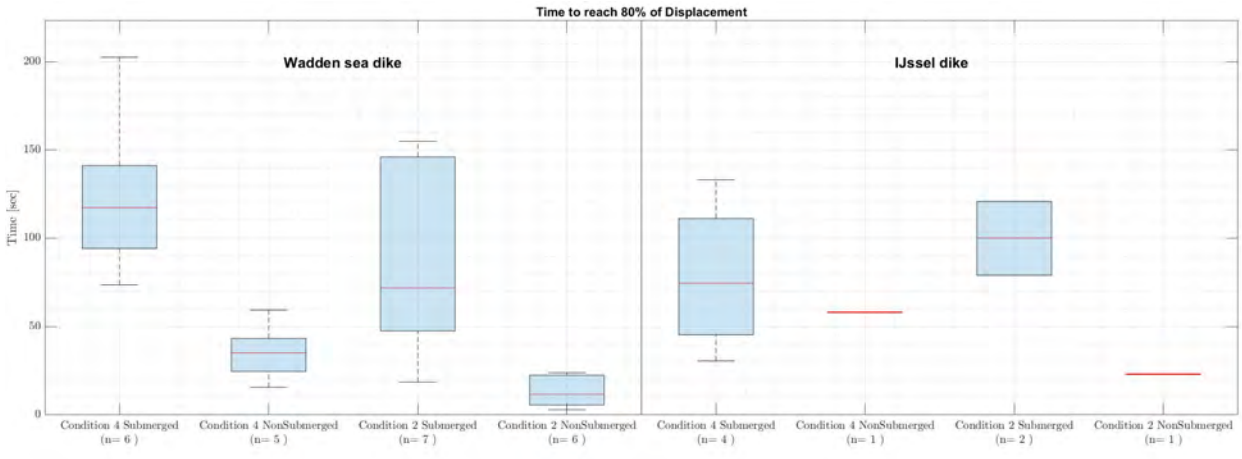

Figure 4.2: Comparison of time to reach 80% of final displacement between submerged and non submerged conditions under constant loading.

It appeared from Figure 4.2 that the time to reach 80% of final displacement was affected by the degree of saturation. However, the scatter around the medians is quit high. This could be explained by the variability of the elasticity modulus E of the grass cover. Furthermore, the flaws in the test execution introduce discrepancies in the growth of displacement. Only the first load block of 600 seconds was considered for the analysis of the displacement rate. The second load block was not considered because the majority of the samples did not reach a constant displacement after increasing the load over 0.3 kN. Therefore, the displacement rate was assumed to be influenced by other processes rather than showing behaviour due to dissipation of matric suction in grass sod. Moreover, it was assumed that large deformations influence the hydraulic conductivity of the grass cover.

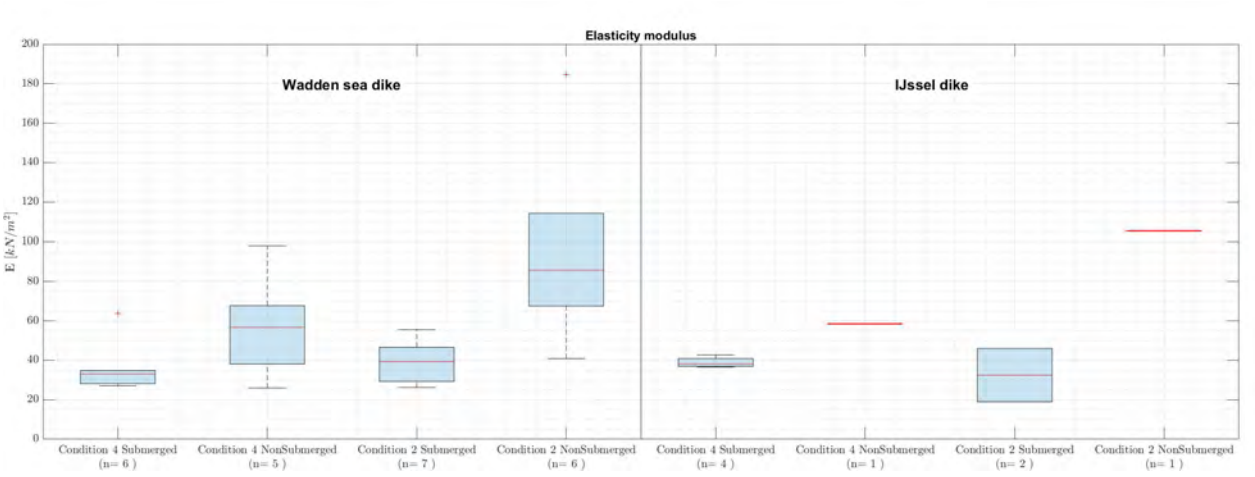

Figure 4.3: Comparison of the elasticity modulus E of the grass sod after an approximately constant deformation of the grass sod was reached.

The results depicted in Figure 4.3 show that the degree of saturation also influences the value of E of the grass cover specimen. Moreover, loading grass covers with higher loads did lead to an ongoing deformation. A decrease of the stiffness with an increasing load level during tests was observed as well, see Figure 4.1. These observations indicate that not only the time to allow drainage of negative pore pressures determine deformation of grass covers due to tensile load, but other processes are involved as well.

4.2. Influence of grass roots on grass cover behaviour

To determine to what extend the failure mode of grass covers is influenced by the tested variables, the dimensions of the grass sod after the sod was lifted out the grass cover were compared for the different test variables.

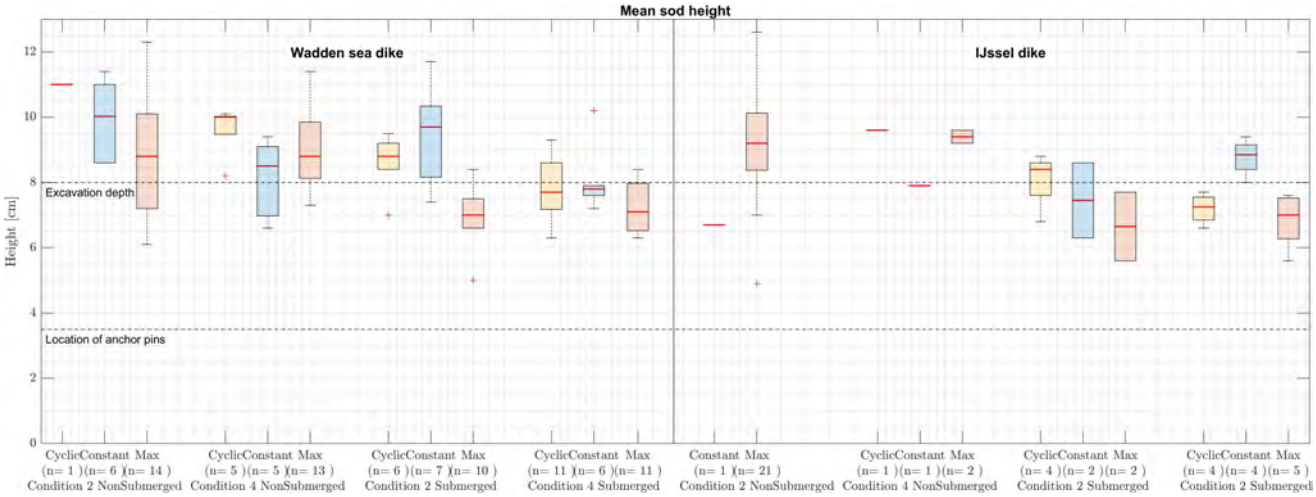

Figure 4.4: Comparison of the height of the grass sod after the sod was lifted out the grass cover.

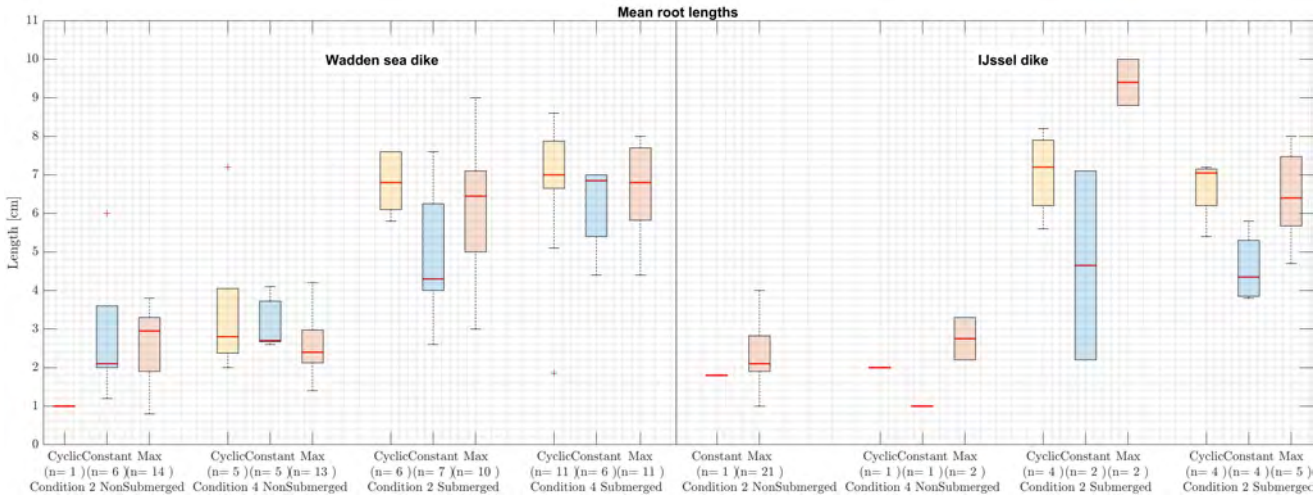

Figure 4.5: Comparison of the mean root length of the grass sod after the sod was lifted out the grass cover.

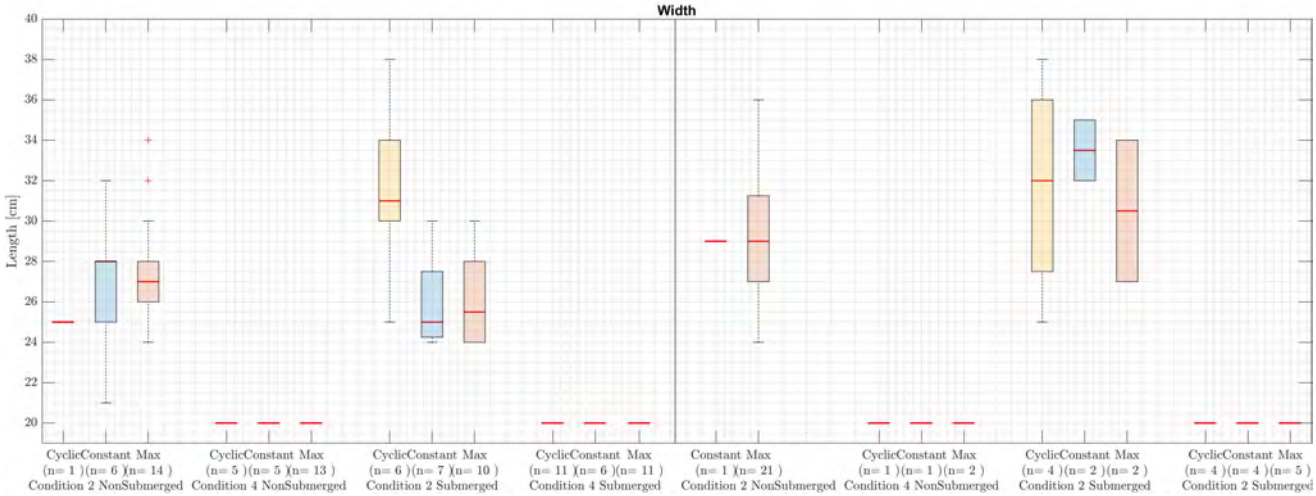

Figure 4.6: Comparison of the mean width of the grass sod after the sod was lifted out the grass cover.

From Figure 4.4 and 4.5 can be concluded that the degree of saturation influences the failure mode of the roots. These results suggest that submerged conditions result in development of the failure plane at less depth, resulting in lower height of the lifted out grass sod sample. Furthermore, the root length was considerably larger for grass sod specimen tested under submerged conditions. Based on the longer root lengths, it is assumed that a larger portion of the roots fail due to slipping under submerged conditions in comparison with the non submerged conditions. This can be explained by a decrease in shear stress between the subsoil and the roots due to submerged conditions. This process possibly influences the location of development of the failure plane as well. For both submerged and non submerged conditions the typical Load - Displacement graphs show a gradual decrease of the resistance by increasing displacement after reaching the maximum strength. This indicates that not all roots break simultaneously. In case of failure due to slipping of the roots, the roots still provide resistance against the tensile load during slipping through the subsoil. Figure 4.7 shows typical examples of Load - Displacement graphs.

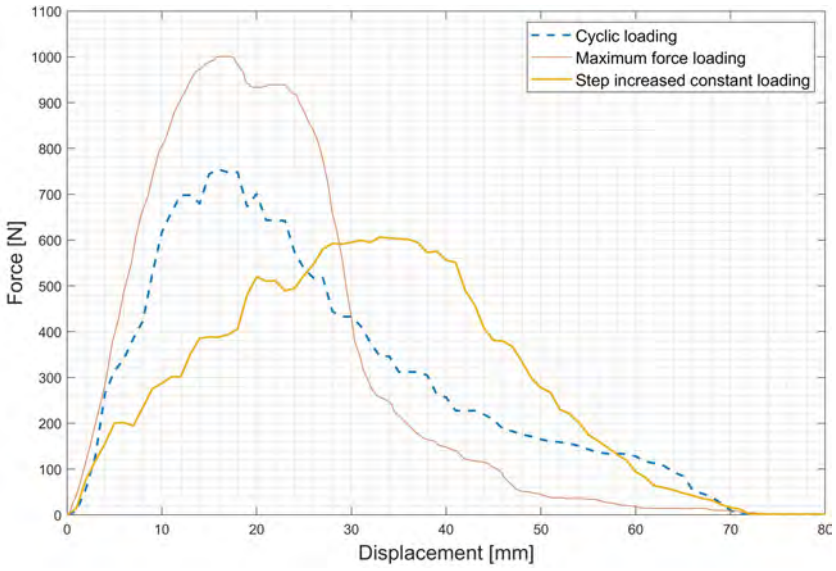

Figure 4.7: Typical Force - Displacement curve for the three different load regimes. The stepwise increased constant load and the cyclic load were force controlled and the maximum force load was displacement - controlled.

The Load - Displacement graph in Figure 4.7 and the displacement at failure of the grass cover in Figure 4.8 indicate that the failure process is influenced by the load regime as well. Figure 4.8 shows that loading at lower load levels enables the grass cover to provide resistance up to a larger displacement. This effect is larger for grass cover samples tested under submerged conditions. This is in line with the interpretation that a larger portion of the roots fail due to slipping rather than breaking under submerged conditions.

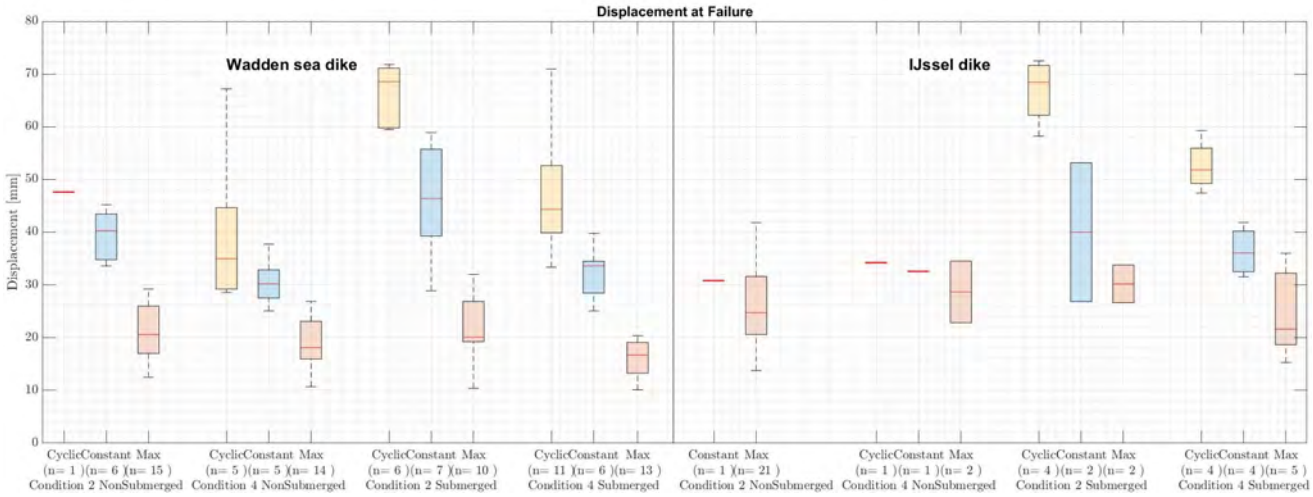

Figure 4.8: Comparison of the displacement at failure of the grass cover sample for the different test variables.

The typical shape of the grass cover sample that is lifted out of the grass cover shows small heights at the edges. The height is increasing towards the middle of the grass sod. The height of the edges of the tested grass sod specimen is smaller or equal to the maximum excavation depth aside the sample. This part of the grass cover is excavated in order to anchor the pull frame. An example is shown in Figure 4.9 and 4.10.

Figure 4.9: Picture of grass cover after the specimen was lifted out of the grass cover. The print of the grass sod in the subsoil show that the failure plane attaches to the maximum excavation depth necessary to anchor the pull frame.

Figure 4.10: Picture of grass sod specimen after it was lifted out of the grass cover. The typical shape of the grass sod shows small heights at the edges increasing towards the middle of the grass sod.

The failure plane in lateral direction is charaterised by small widths at the edge of the grass cover sample. The width increases towards the center of the sample. The failure plane starts generally at the edge where the sample and the adjecent grass cover intersect. This is at a width of $20\,cm$. An example is shown in Figure 4.11 and 4.12. The location where the horizontal failure plane develops seems to be influenced by the grass cover quality and the subsoil type, see Figure 4.6. However, it is hard to determine the influence of the tested variables due to large variability in width of the grass cover samples.

Figure 4.11: Picture of grass cover after the specimen was lifted out of the grass cover. The print of the grass sod in the subsoil shows that the failure plane attaches to the adjacent grass cover at the location of the edge of the grass cover sample.

Figure 4.12: Picture of grass sod specimen after it was lifted out of the grass cover. The typical shape of the grass sod shows widths of circa $20\,cm$ at the edges increasing towards the centre of the grass cover sample.

The correspondence between the location of the edges of the failure plane and the dimensions of the excavation indicate that the location of the failure plane is influenced by the method and sample preparation. This indicates that stress concentration at the edges cause initiation of the failure plane. This applies for both the horizontal and the vertical direction.

4.3. Fatigue of the grass cover

To determine whether damage accumulation occurs, the load at failure of the grass sod for three different load regimes as described in section 3.1 were compared.

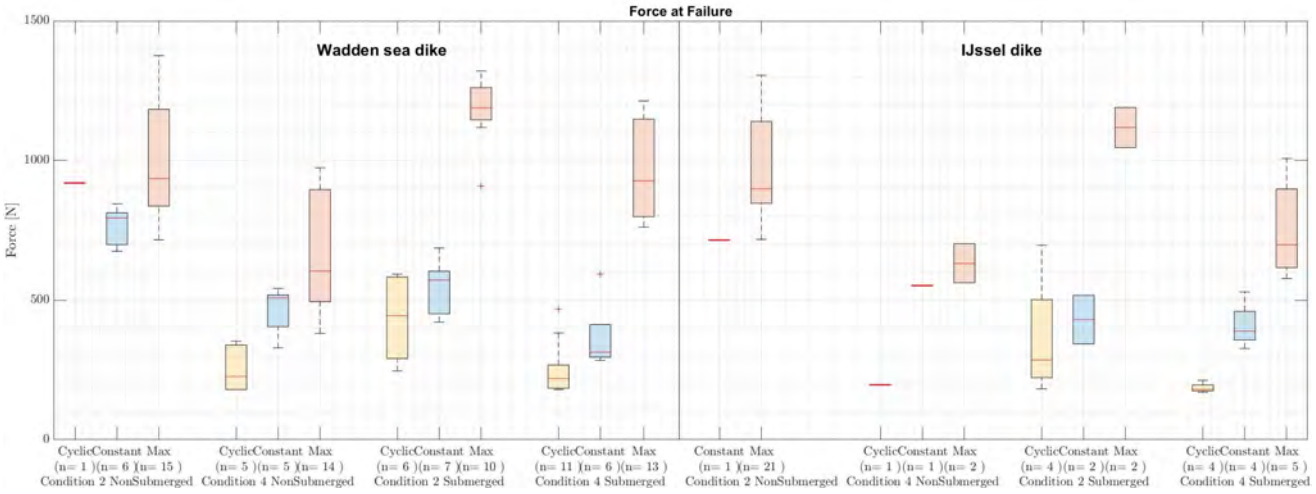

Figure 4.13: Comparison of the load that causes failure of the grass cover between Cyclic loading, Constant loading and Maximum force loading.

The results depicted in Figure 4.13, suggest indeed the occurrence of damage accumulation. Especially repetitive loading causes failure at lower load levels in comparison with the static strength determined by a maximum force load. To gain more insight into the process of damage accumulation due to repetitive loading, the displacement measurements and the development of elasticity of the grass cover over successive loading cycles were used to evaluate. The displacement and elasticity over successive loading cycles show in general the same trends in all tests. Therefore, a deviation in distinguished phases based on this trends is made. The three different phases are shown in Figure 4.14.

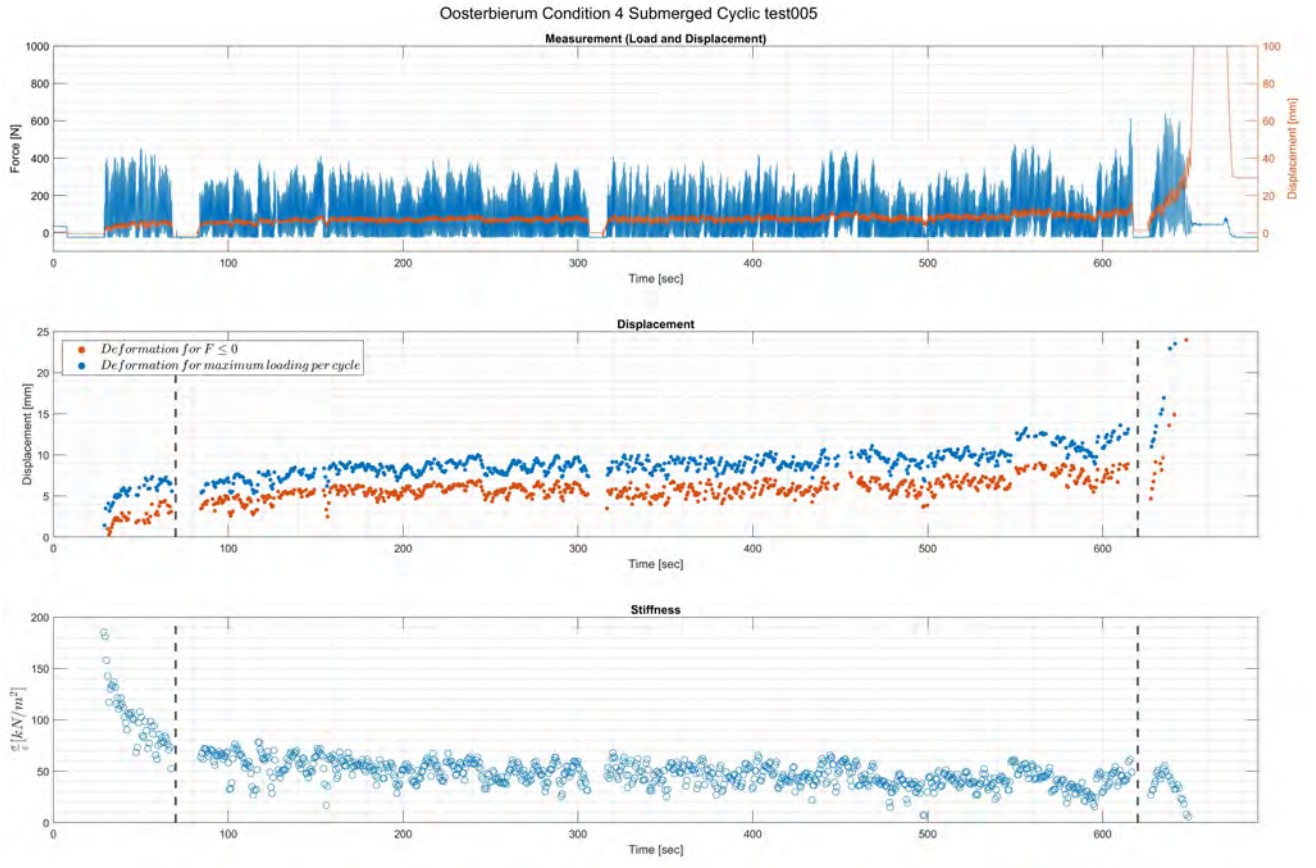

Figure 4.14: Example of typical behaviour under repetitive tension loading. The figure shows the results of cyclic loading during submerged conditions and with four sides cut loose. The top panel shows the raw measurement of force and displacement. The center panel shows the maxima and minima of the measured displacement per cycle. The lower panel depicts the elasticity for each load cycle. The variables are shown as a function of time.

In the first phase, a rapid increase in displacement and a rapid decrease of elasticity is observed. In the second phase the displacement grows with a low and stable rate and the elasticity of the specimen decreases with a low and stable rate. After a load cycle, the grass sod does not return to the initial position. This results in a residual displacement as shown by the red dots in the center panel of Figure 4.14 and 4.15. This residual displacement is described in depth in the next section. During the last phase, the displacement growth increases and the elasticity of the test specimen decreases rapidly until failure of the grass cover specimen.

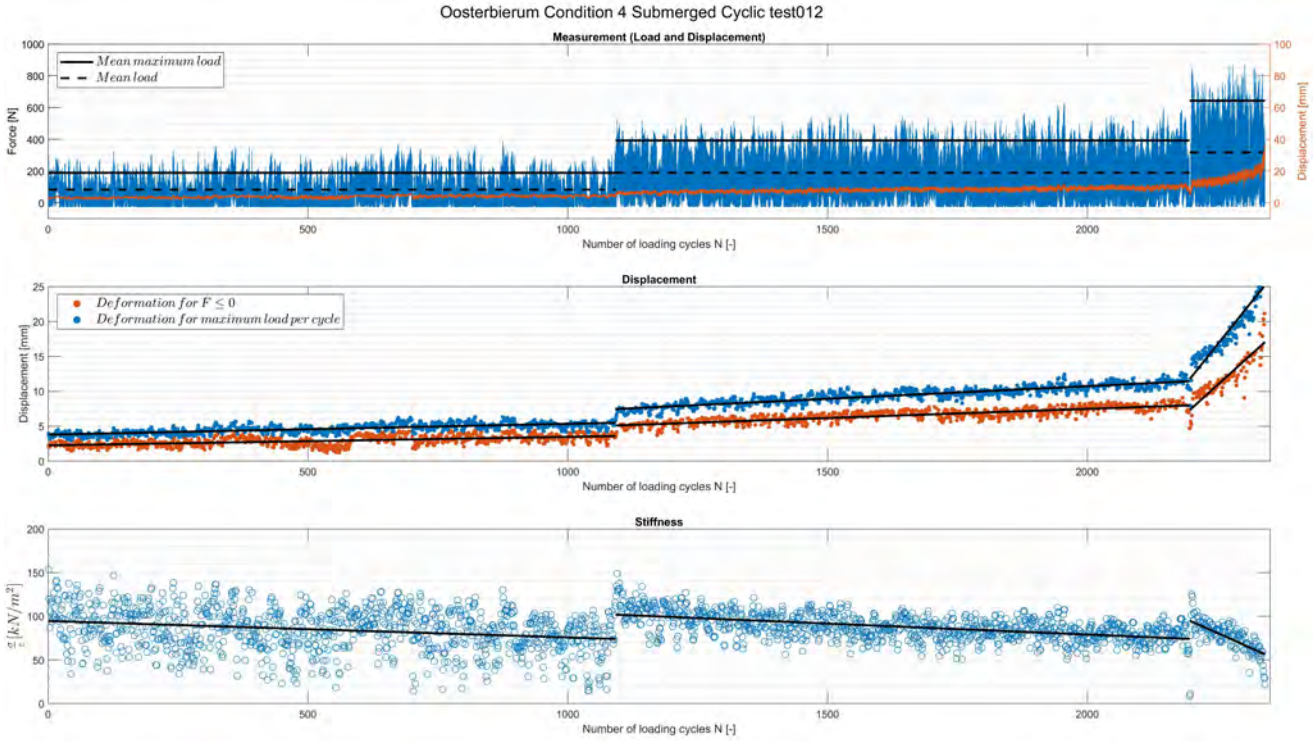

Figure 4.15: Example of typical behaviour under repetitive tension loading. The figure shows a change in inclination of the trend line in displacement and stiffness due to increase of the load. Linear line was fit to the data with standard linear regression functions available in *MATLAB R2019a*.

During the first and second phase considerable scatter of the stiffness was observed for the strong specimen, i.e. specimen that were able to withstand multiple and large loading levels. This effect is shown in the lower panel of Figure 4.15. The specimen also showed a dependency between the inclination of the trend line of displacement and elasticity and the load magnitude. The inclination of the trend line describing the development of the displacement increases after increasing of the load magnitude. This results in a decrease of the elasticity as well. An example of this process is given in Figure 4.15. The relation between the inclination of the trend line and the load magnitude is shown in Figure 4.16.

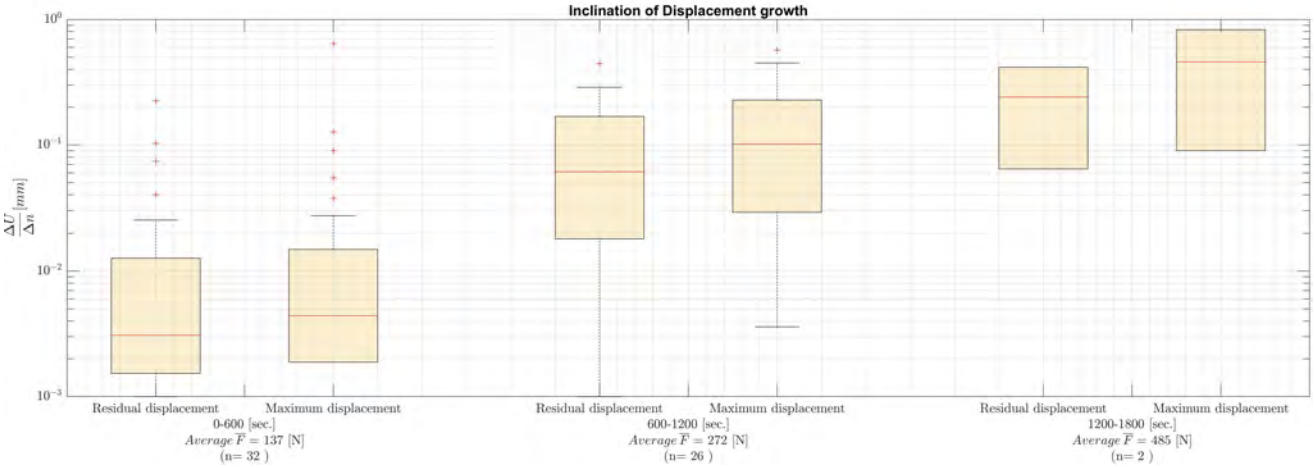

Figure 4.16: The inclination of the trend line describing the development of displacement per load block of circa 600 seconds in relation with the magnitude of the imposed cyclic load. The magnitude is described by the average of the mean load per test as indicated in the center panel of Figure 4.15. The grass cover specimens showed a variation in strength. Thereby grass cover specimen failed at different load levels. This resulted in a decrease in the sample size n with increasing test duration.

4.3.1. Elastic - plastic behaviour

To determine if the grass cover deformation behaves elastic - plastic and exhibits a clear distinction between the elastic and the plastic range of deformation, the grass cover behaviour under cyclic tensile loading was analysed in detail. Figure 4.17 shows the development of the Load - Displacement relation over successive load cycles. The detailed measurement of the displacement in the lower panels of Figure 4.17 shows a clear combination of plastic and elastic deformation. After the first load cycle, indicated with t1, the grass sod does not return to the initial position resulting in a residual displacement. This indicates plastic deformation. The trajectory between the maximum deformation during one load cycle and the residual deformation is considered as elastic deformation. The first load results in a relative large residual displacement. After the first load, an increasing number of successive load cycles results in growth of the residual displacement at a relative stable rate as shown in Figure 4.15 and the lower panels of Figure 4.17. However, limited time between successive load cycles prevent the grass sod to return to the initial position after loading, so the residual displacement is preserved. An increase in time between successive loading cycles enables the grass sod to return to the initial position as shown by the measurements between time t2 and t3, presented in the top panel of Figure 4.17. Nevertheless, loading after reaching the initial displacement results almost instantaneously in the same behaviour as before reaching the initial displacement. This is shown by t2 and t3 in the Load - Displacement relation in the lower left panel of Figure 4.17. The part of displacement indicated as residual deformation provides limited or no resistance against deformation. Therefore, the residual displacement is assumed to be the result of plastic deformation of the grass cover.

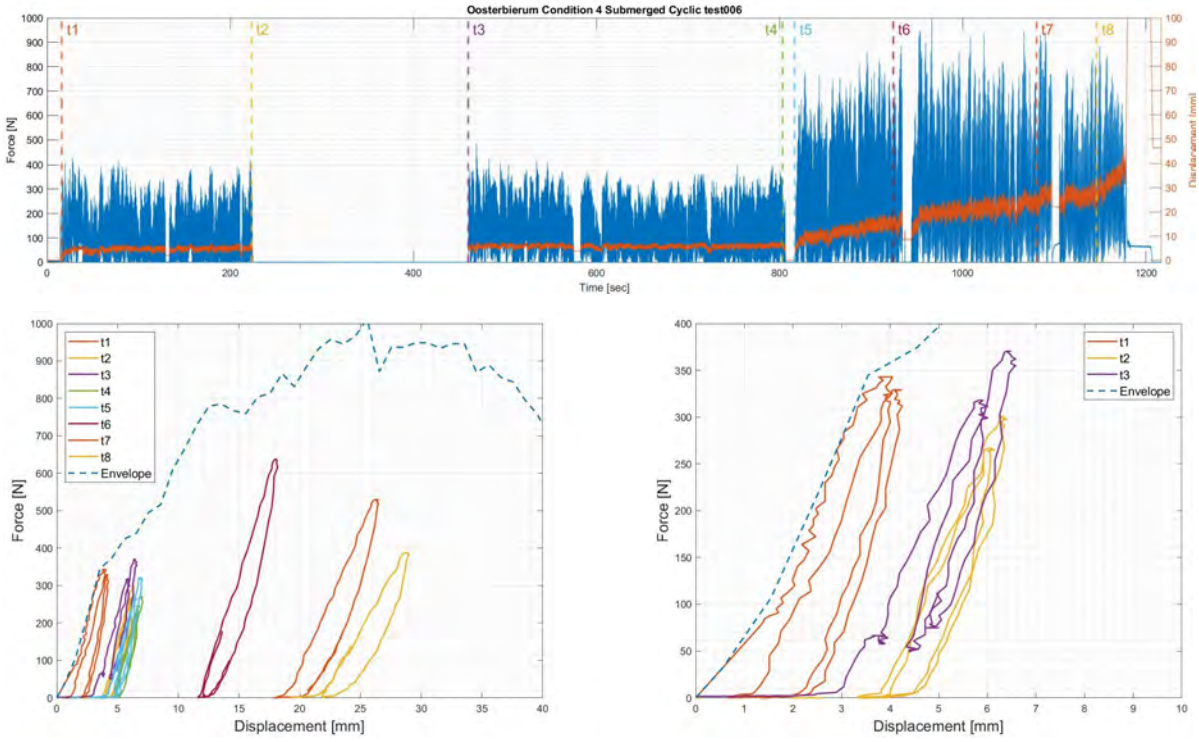

Figure 4.17: Development of Load - Displacement relation over successive loading cycles. The graphs in the lower panels show the Load - Displacement relation at points in time as indicated in the top panel. The envelope of the total the Load - Displacement relation is depicted as well. The lower right panel shows a close-up of the t1 until t3 and points out the effect of an increased time between successive loading cycles.

With an increasing number of successive load cycles, the portion of plastic deformation increases. Up to t4, the increase of the plastic deformation barely influences the inclination of the Load - Displacement relation of the elastic part of the deformation. Nevertheless, the increase of plastic deformation results in a decrease of the total elasticity. Figure 4.18 shows a clear difference in total elasticity and partial elasticity of the tested grass sod sample. Total stiffness and partial stiffness were defined in Section 3.3. As mentioned before, an increase in load results in a higher growth rate of the residual displacement but also in a larger decrease in both total and partial stiffness.

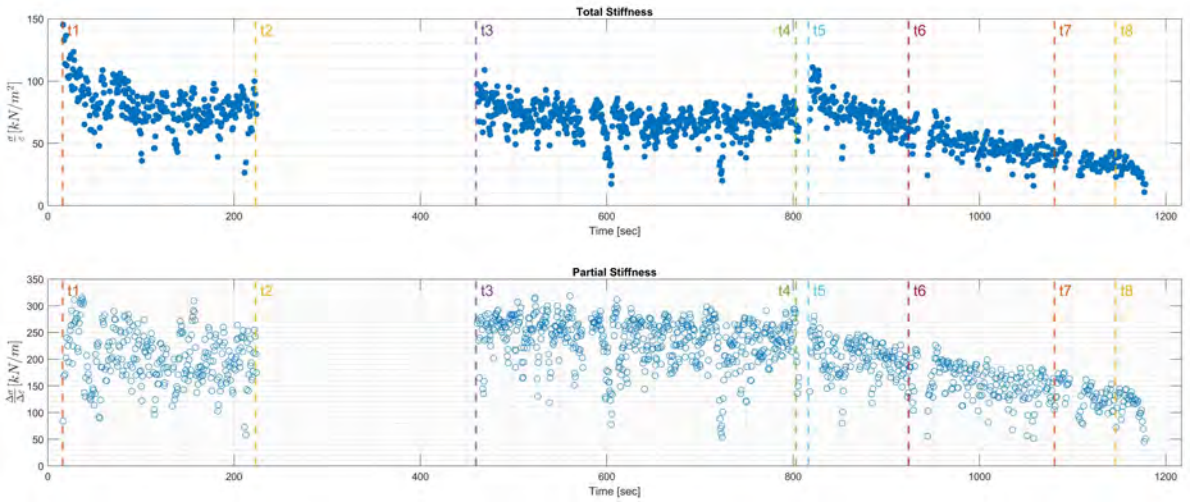

Figure 4.18: Development of total and partial stiffness as defined in section 3.3.

Based on the results, it is not possible to determine a difference in behaviour between submerged and non submerged conditions. This is caused by the large variation in induced load due to the manual control of the grass pull device. Therefore, it remains unclear whether occurrence of negative pore pressure during cyclic loading influences the behaviour of the grass cover. However, flaws in the execution of several tests caused extreme peak loads, which did not lead to extreme deformation of the grass sod. This indicates a time dependency of the deformation. This might indicate development of negative pore pressures in the grass cover.

In comparison with the cyclically loaded grass cover sample, the grass cover under stepwise increased constant load behaves less stiff whereby an ongoing deformation during constant load was observed. The deformation is characterised by a decrease in displacement rate up to a more or less constant value under low load levels. This effect is shown in Figure 4.19.

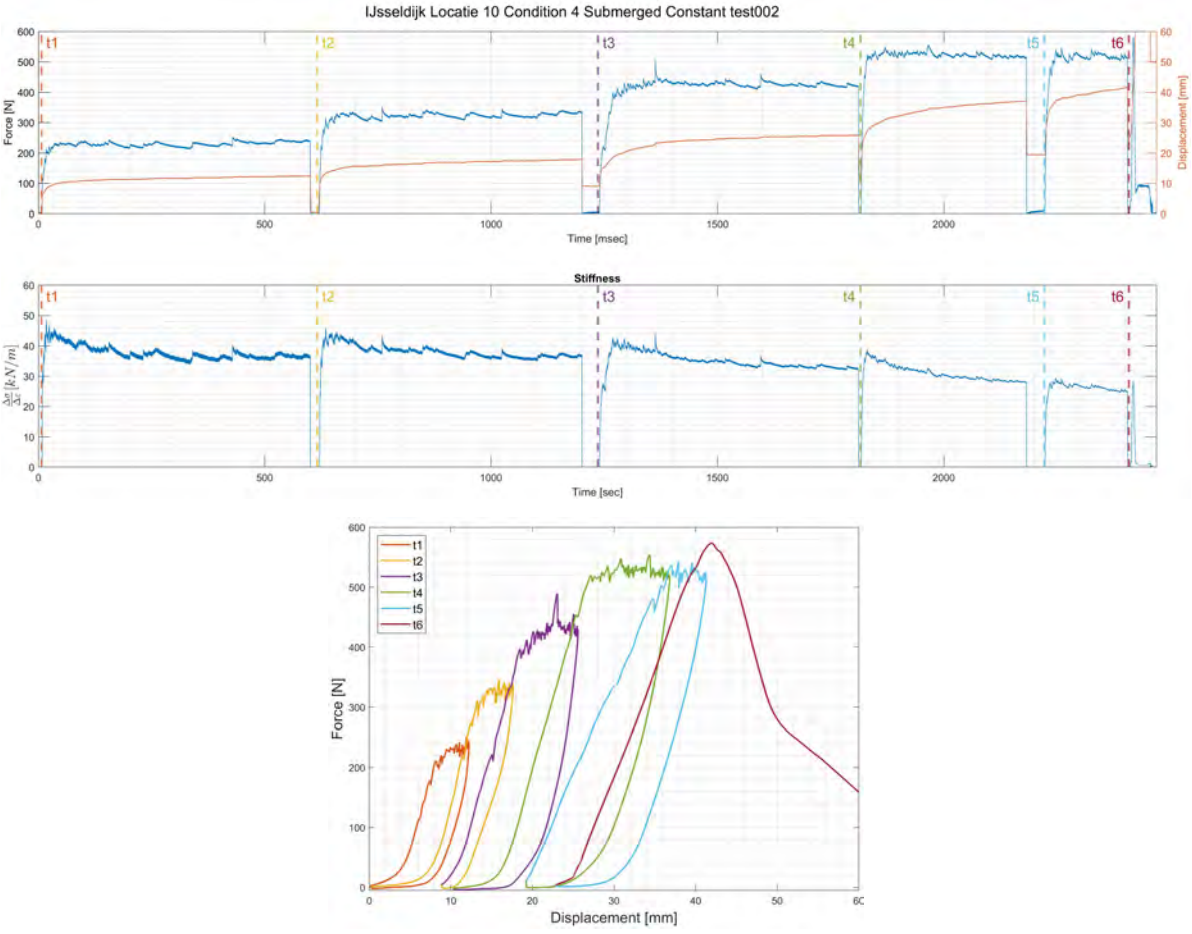

Figure 4.19: The results of stepwise increased constant load during submerged conditions and with four sides cut loose. The development of displacement and stiffness are shown as a function of time. The results show the effect of unloading of the grass sod before increasing the load. The graphs in the lower panel show the development of Load - Displacement relation over successive loadings. The Load - Displacement relation between points in time is indicated with colors. The colors are in corresponds with the colors in the top panel.

The grass cover behaviour under stepwise increased constant load also shows similarities with the behaviour of the grass cover sample under cyclic loading. An increase in time between successive loading blocks enables the grass cover sample at first to return to the initial position. After reaching a certain displacement, the grass cover sample was unable to return to the initial position. An example is shown in Figure 4.19. Loading after reaching the initial displacement, results almost instantaneously in the same behaviour as before reaching the initial displacement. The Load - Displacement relation depicted in lower panel of Figure 4.19 shows a decrease of resistance to deformation during the first part of displacement over successive loading.

Attempts were made to determine a transition point between elastic and plastic deformation. First, an attempt was made to determine this point based on analysis of the deformation of the grass cover due to stepwise increased constant load and cyclic loading. The second attempt to determine the transition point was based on the method described by Hallett and Newson (2005). Neither of the attempts did provide a transition point between elastic and plastic deformation nor a fatigue limit. Nevertheless, grass covers under stepwise increased constant load reached a stable stiffness at low loading levels. But deformation up to this constant level did not only consist of elastic deformation. However, the stable growth of the plastic deformation in combination with the relation between the load magnitude and the growth rate makes the development of damage accumulation predictable. The predictable process of the damage accumulation process provides the possibility to attribute normative values to the growth rate of the plastic deformation due to cyclic loading.

5

Proposed Method

For a good and effective dike management, a simple method to determine the erosion resistance provided by grass covers is desired. Based on the revealed insights into the mechanical behaviour of grass covers found in this study and described in Chapter 4, a method to determine the grass cover resistance to repetitive loading is proposed.

Test results show that grass covers are subject to fatigue. The strength of the grass cover is to a great extent determined by the load history. Repetitively loaded grass cover samples failed at stress levels far below the static strength. These findings in combination with the cyclic nature of loads induced by overtopping waves emphasize the importance of assessment of the erosion resistance of grass cover based on the process of damage accumulation. The proposed method provides a procedure to estimate parameters to describes the process of damage accumulation in the grass cover by means of direct pull test executed with the grass sod pull device.

This relative simple and time efficient method enables to asses the erosion resistance of a grass cover on specific dike sections based on physical processes that determine the mechanical behaviour of the grass cover. The time efficiency of this method makes it feasible to test a large number of grass cover samples. As a result, this method allows for a good estimation of the variability of the strength of the grass cover on a dike section.

5.1. Method to estimate fatigue limit

The test results showed that the fatigue process is characterised by a constant growth rate of plastic deformation. Furthermore, the results show that the magnitude of growth rate is determined by the magnitude of the load. This method combines these characteristics of the fatigue processes, the maximum deformation of the grass cover and the estimated number of overtopping waves to estimate the maximum allowable growth rate of plastic deformation. The magnitude of the load that induces the maximum allowable growth rate provides an estimation of the fatigue limit.

The fatigue limit of the grass cover is estimated by means of a direct pull test. The test set-up of the sod pulling test consists of a small pull frame with dimensions of $20 \times 20\,cm^2$, see Figure 3.1, and a computer controlled pulling device. The computer controlled pulling device is able to induce an prescribed load regime on grass cover samples. The prescribed sample preparation for the method is based on the revealed influence of the test condition on the mechanical behaviour of the grass cover.

Grass cover sample preparation

To estimate the fatigue limit of the grass cover, a grass cover sample of $20 \times 20\,cm^2$ cut at four opposite sides is tested. An example is shown in Figure 5.4 (b). The sample is cut to a depth of $20\,cm$ to minimize the influence of the adjacent subsoil to the formation of the failure plane. The pull frame is anchored with 5 pins at a depth of $3.5\,cm$. The test is executed under submerged conditions to ensure the correct failure mode is tested. The submerged conditions are provided by a box of $80 \times 40 \times 20\,cm$ (Length x Width x Height). The box is installed over the anchored pull frame and hammered partly into the soil. An example is given in Figure 3.7. The box is filled with water 30 minutes before executing the test to ensure complete saturation of the grass cover on dike section.

Stepwise increased cyclic load
The growth rate of the plastic deformation of the grass cover due to cyclic loading, see Section 4.3, is used as measure of the grass cover fatigue strength. The maximum allowable growth rate is determined based on the expected number of overtopping waves at a specific location and the deformation of the grass cover at failure found in a pulling test. The force that results in the maximum allowable growth rate is found by inducing a stepwise increased cyclic load. The proposed load regime is depicted in Figure 5.1.

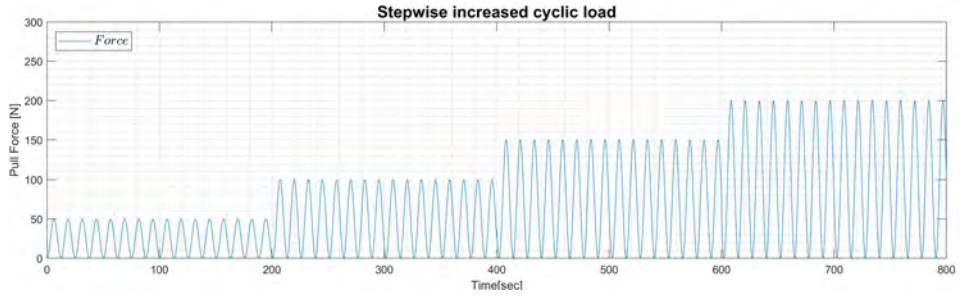

Figure 5.1: During cyclic loading, the grass sod is repetitively loaded with a constant period of $0.5\,Hz$ and a stepwise increased amplitude. The amplitude of the load increases every 100 cycles with $50\,N$, starting with a load of $50\,N$. This process proceeds until failure occurs.

Based on the nature of the damage accumulation process, it is assumed that 100 load cycles are sufficient to determine the relation between the growth rate and the magnitude of the force. The displacement at failure is found by stepwise increasing the cyclic load until failure occurs. The specimen is tested at a frequency of $0.5\,Hz$. The test results in a value of displacement at failure $U_{max}\,[mm]$ and a relation between growth rate $\frac{\Delta U}{N}\,[mm]$ and load magnitude $F\,[N]$. Based on the estimated number of overtopping waves $\tilde{N}_{waves}$ and U_{max}, the maximum allowable growth rate $\left(\frac{\Delta U}{N}\right)_{max}$ is determined according to Equation 5.1.

$$\left(\frac{\Delta U}{N}\right) = \frac{U_{max}}{\tilde{N}_{waves}}\,[mm] \tag{5.1}$$

The load magnitude $F\,[N]$ that leads to the maximum allowable growth rate is assumed to be an estimation of the fatigue limit $\tilde{S}_0\,[N/m^2]$ of the grass cover sample.

Number of tests
For assessment of the grass cover of a dike section, the dike section should be divided in segments based on variability of resistance against loads and variability in the expected loads. The spatial variability of $\tilde{S}_0$ within a dike section is expected to be determined by soil type, orientation of the dike and maintenance of the grass cover. Within the normative segments, the required number of tests within a segment of a dike section is determined by the found variability of $\tilde{S}_0$.

5.2. Relation with hydraulic load

With the grass pulling test, the strength of the grass cover is quantified in a lift force instead of a hydraulic load as used in the current grass cover assessment methodology. In order to relate the value of $\tilde{S}_0$ to hydraulic loads, two approaches are available. The first approach is to empirically relate $\tilde{S}_0$ to the results of the tests with the wave overtopping simulator. This approach requires a substantial amount of test results of both tests to construct a reliable relation between the two tests. The second approach is to determine the hydraulic characteristics of overtopping waves that result in stress development equal to the found value of $\tilde{S}_0$. The hydraulic characteristics of overtopping waves can be determined by models describing the stress development based on physical processes, e.g. a model based on continuum behaviour of porous media (Van Damme, 2019) or discrete element model describing particle-particle interactions as described by Helmons and Van Rhee (2019). Both types of models require a description of the mechanical behaviour of the grass sod (Van Damme, 2019). The required input parameters are the elasticity modulus (E), the shear modulus (G) and the hydraulic conductivity (k_s). A method to determine E and k_s of the grass sod, appropriate to serve as input for this model and describe the grass sod behaviour under tensile loading, is proposed in the following section. In addition, an approach to determine G is suggested.

5.2.1. Method to determine grass cover parameters E and k_s

Deformation of grass covers due to tensile loading is a time dependent process as shown in Section 4.1. For small deformation, the time dependency is assumed to be related to a combination of elasticy of the porous material and dissipation of pore water pressure. Therefore, the deformation of grass covers under tensile load is assumed to be an inverse consolidation process. Parameters describing this process are E and k_s (Winterwerp and Van Kesteren, 2004). To determine E and k_s a solution of Terzaghi's problem (1948), describing the one-dimensional case of flow and deformation of porous material as described by Verruijt (2010), is applied. Figure 5.2 depicts the considered system.

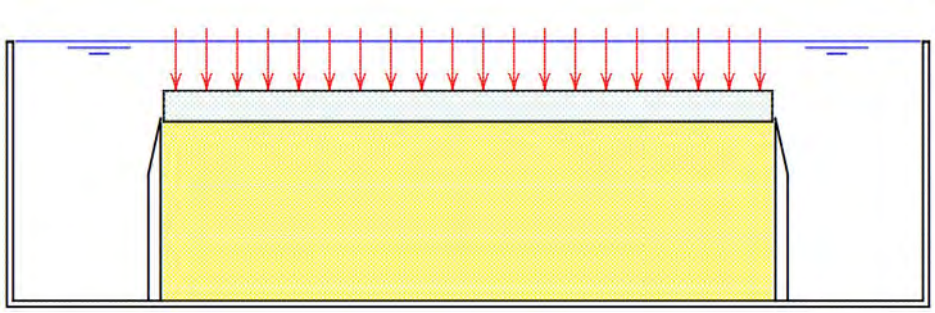

Figure 5.2: The one-dimensional case of flow and deformation in the vertical direction only. Reprinted from Verruijt (2010).

According to (Verruijt, 2010), the one-dimensional consolidation is described by the following differential equation:

$$\frac{\partial \varepsilon}{\partial t} = -m_v \frac{\partial \sigma_{zz}}{\partial t} = \alpha m_v \frac{\partial p}{\partial t} \tag{5.2}$$

Where ε is the volume strain, m_v is the vertical compressibility of a laterally confined soil sample, σ the total stress and P the pore water pressure. Terzaghi (1925) showed that in case of zero lateral deformation and constant vertical total stress the consolidation equations simplify to (Verruijt, 2010):

$$\frac{\partial P}{\partial t} = c_v \frac{\partial^2 P}{\partial z^2} \tag{5.3}$$

Where c_v denotes the consolidation coefficient.

Verruijt (2010) provides an adequate solution of the consolidation problem to determine the displacement of the top of the sample. The solution as described by Equation 5.5 gives an expression for the degree of consolidation (C) as a function of time. The degree of consolidation C is defined as:

$$C = \frac{u - U_0}{U_\infty - U_0} \tag{5.4}$$

Where u denotes displacement, U_0 denotes the immediate displacement and U_∞ denotes the displacement after complete dissipation of the pore pressures.

$$C = 1 - \frac{8}{\pi^2} \sum_{j=1}^{\infty} \frac{1}{(2j-1)^2} e^{-(2j-1)^2 \frac{\pi^2}{4} \frac{c_v t}{h^2}} \tag{5.5}$$

with:

$$c_v = \frac{k_s}{\left(\alpha^2 \frac{1}{E} + S_p\right) \gamma_w} \text{ simplified to } c_v = \frac{k_s}{\frac{1}{E} \gamma_w} \tag{5.6}$$

Where h is half of the layer of thickness of the sample, γ_w denotes the density of water. The assumption of incompressible fluid and the solid particles give $S_p = 0$. By multiplying the degree of consolidation with the final displacement, the progress of deformation over time is estimated.

The values of E and k_s are estimated based on the results of a submerged constant load pulling test. The test set-up and sample preparation for the test to estimate the values of E and k_s are identical to the sample preparation of test to estimate the fatigue limit and described in Section 5.1. The final displacement U_∞ of the grass cover is found by inducing a constant load of $100\,N$. The time necessary to reach the final deformation is determined by the hydraulic conductivity of the subsoil. Based on the experiences gained during this research, this time is approximately 15 minutes. The value of E is determined based on the final displacement due to the induced load according to Equation 5.7.

$$E = \frac{\sigma}{\varepsilon_\infty} \tag{5.7}$$

Where stress (σ) and final strain (ε_∞) are determined based on the dimensions of the sod as measured after the sod was lifted out the grass cover. The formulae to determine stress and strain are shown in Equation 5.8.

$$\begin{aligned} \sigma &= \frac{Force}{Width\,of\,pull\,frame \times Width\,of\,grass\,sod} \\ \varepsilon_\infty &= \frac{Final\,displacement}{Mean\,height\,of\,pulled\,out\,sod} \end{aligned} \tag{5.8}$$

The value of k_s is estimated by fitting the results of the solution of Terzaghi's problem to the results of of the submerged constant loading test. An example of this method is given in Figure 5.3

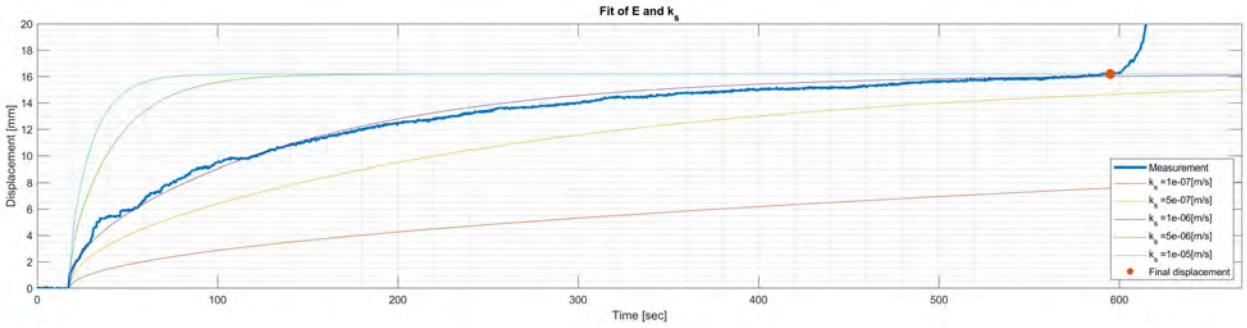

Figure 5.3: Example of method to determine E and k_s, applying the expression for degree of consolidation as described by Verruijt (2010). For this example the results of the submerged stepwise increased load regime, as described in Section 3.2, were used as input. Please note that the induced load is not in agreement with the load as proposed.

5.2.2. Method to determine grass cover parameter G

Grass is a non-isotropic material (Muijs, 1999). To be able to model the mechanical behaviour of grass covers, both the elasticity modulus (E) and the shear modulus (G) are required. Insight into the grass cover strength in lateral directions is determined by a submerged constant load pulling test. The test set-up and load regime to estimate the values of G is identical to the test set-up to estimate E and k_s. The sample preparation on the other hand differs from the sample preparation to estimate E and k_s.

To estimate G, samples with two sides cut are tested. The grass cover sample of $60 \times 20\,cm^2$ is cut at 2 opposite sides up to a depth of $20\,cm$. In Figure 5.4 examples of a grass cover samples are shown. The grass cover is also cut loose in vertical direction at a depth of $10\,cm$ to eliminate the influence of grass roots in vertical direction. The cut plane has dimension of $20 \times 20\,cm^2$. The location of the cut plane is indicated in red in Figure 5.4. Submerged conditions are provided by a box of $80 \times 60 \times 20\,cm$ (Length x Width x Height). The shear modulus is calculated by the final displacement due to the induced load according to Equation 5.7.

$$G = \frac{\sigma}{\varepsilon_\infty} \tag{5.9}$$

The formulae to determine stress and strain are shown in Equation 5.8.

(a) *Two sides cut loose.* (b) Four sides cut loose.

Figure 5.4: Location and dimensions of cuts for grass cover samples with two and four sides cut loose.

The grass parameters determined by the proposed method provide necessary input for computational models that calculate the stress development in the grass cover induced by overtopping waves. These models in combination with the estimation of the fatigue limit $\tilde{S}_0$ provide an useful tool to assess the erosion resistance of grass covers on dikes.

6

Discussion

The material behaviour of grass sods is essential in understanding the resistance of grass covers loaded by overtopping waves. To gain more insights the influence of 1.) Tensile behaviour of cohesive sediments, 2.) Tensile behaviour of grass roots, and 3.) Fatigue of the grass cover, the mechanical behaviour of grass cover was tested. In this chapter a critical reflection and evaluation of the results presented in the previous chapter is made. This chapter is split into four sections. First, results regarding the hypothesised processes are discussed. Second, the proposed method to estimate the fatigue limit of the grass cover is discussed. Third, the limitations and disturbances of the applied field test method are discussed. Fourth, an interpretation of outcomes in relation with wave overtopping is made.

6.1. Influence processes on behaviour of the grass cover

In the next section, the test results of the test executed in order to gain insight in the possible effect of the in section 2.6 hypothesised physical processes are discussed.

Behaviour due to tensile strength of cohesive material

To test the occurrence and influence of development and drainage of negative pore water pressure in the grass sod without measuring pore pressures, the behaviour of the grass sod under stepwise increased constant load for submerged and non submerged conditions was evaluated. The results of the analysis of the displacement rate due to a constant tensile load show indeed a influence of the degree of saturation. The results presented in Figure 4.2 show that the time to reach 80% of the final displacement was considerably longer for tests conducted under submerged conditions compared to the tests conducted under non submerged conditions. This indicates that the time dependent process of development and drainage of negative pore pressures, associated with deformation of porous media due to tensile loading, influences the mechanical behaviour of the grass cover. These results are in agreement with tensile behaviour of cohesive materials as described by Winterwerp and Van Kesteren (2004) and Tollenaar et al. (2017). Based on this finding, it can be implied that that computation of the elasticity modulus E of the grass sod should be based on a long-lasting load. Inducing large and ongoing deformation rates results in a description of combined processes. Therefore, a difference between the perceived elasticity and the elasticity modulus E of the grass cover should be made. Figure 4.1 shows an example of the difference between the concurrent perceived elasticity of the grass cover and E of the grass cover.

In addition, the test results indicate that the degree of saturation influences other processes as well. The results depicted in Figure 4.3 show that the degree of saturation also influences the E of the grass cover specimen. Moreover, loading grass covers with higher loads did lead to an ongoing deformation. In addition, a decrease of the elasticity with an increasing load level was observed as well, see Figure 4.1 and 4.19. Plastic deformation as shown in Figure 4.19 occurred as well. These observations indicate that not only the time to allow drainage of negative pore pressures determine deformation of grass covers due to tensile loading, as expected on mechanics of porous media (Verruijt, 2010). The test results show that other processes are involved as well. This is explained by findings of Hallett and Newson (2005), who showed that mechanical properties of clay change due to tensile loading. Therefore, it is assumed that the material characteristics of the grass cover change with an increase in deformation. This results in a change of mechanical properties.

These findings show that describing the mechanical behaviour of the grass cover by only considering dissipation of negative pore pressure parametrized by a constant value of E and k_s at higher load levels might not be suitable. Based on the test results, it was not possible to determine whether the elasticity modulus E changes over time or that E is a function of the magnitude of tensile stress as well. This was caused by a the short timespan of the tested constant load. The second cause was that a load of a certain magnitude was followed up by a load with an increased magnitude instead of the same magnitude.

Behaviour due to tensile strength of grass roots
To determine to what extent the root strength is influenced by the tested variables, the dimensions of the grass sod, after the sod was lifted out the grass cover were compared for the different test variables. It appeared that the degree of saturation influenced the roots length of the grass cover specimen. Based on these results, it is assumed that a larger portion of the roots fail due to slipping under submerged conditions in comparison with the non submerged conditions. The results are shown in Figure 4.4. This effect was also observed by Pollen (2007). Based on these findings, it can be concluded that testing the grass cover strength should be executed under submerged conditions in order to test the failure mechanism as expected during wave overtopping.

The results in Figure 4.5 show that the height of the grass sod is barely influenced by the test variables. Because of the decay in tensile strength of the grass cover due to a decay in root density with depth, the average height of the tested grass cover specimen was assumed to be a measure for the depth where the tensile stress exceeds the tensile strength. However, based on the typical shape of the tested grass cover specimen, it is assumed that the location of the initiation of the failure plane is influenced by the method. To enable anchoring of the pull frame, the grass cover specimen is excavated to a depth of circa $8\,cm$. The edge of failure plane of the majority of tested grass cover specimen corresponds with the excavation depth. The height increases from the edge to the maximum height of the grass cover specimen. To find the real intersection of tensile stress and strength, the grass sod specimen should be simplified to a one-dimensional system by cutting the edges of the surface over the full depth of the grass cover. This means that the grass cover sample is cut loose from the adjacent grass cover up to a depth of $20\,cm$. The same problem applies for the direction parallel to the slope of the dike cover. To get a better insight in the tensile strength of the grass cover parallel to the slope, the two sides must be cut over a longer distance instead of the distance as shown in Figure 3.8 (a). This results in testing of the grass cover strength in two directions instead of testing a more complicated geometry. The improvements of the cut dimensions lead to more precise results. The improvements in the sample preparation are applied and described in Chapter 5 and depicted in Figure 5.4.

Bijlard (2015) proposed a practical approach to determine the influence of cutting the grass cover necessary to install the pull frame on the maximum strength of the grass cover. This approach is based on the difference in maximum strength of the grass cover specimen cut at four and two sides. By simplifying the grass cover to a two-dimensional and one-dimensional problem, the influence of the cuts may be better determined.

Fatigue of the grass cover
The test results showed the occurrence of damage accumulation. The load history has a large influence on the load necessary to induce failure of the grass cover as shown in Figure 4.13. Based on the test results, no threshold stress level was found below which only elastic deformation was induced. Moreover, the plastic deformation arises form the first load cycle. This outcome is contrary to that of Hallett and Newson (2005) and Tollenaar et al. (2017) who found a clear transition between the elastic range and the plastic range. The only difference between the test methods that can explain the difference in outcomes is the displacement rate. The tested displacement rate in this study $(2\,cm/s)$, is considerably higher than the displacement rate $(1\,mm/min)$ tested by Tollenaar et al. (2017).

This study did not reveal a fatigue limit. However, another possible measure to describe the process of damage accumulation was found. It was found that the plastic deformation was indicated by a residual displacement after the first load cycle as shown in Figure 4.17. Due to this residual displacement a difference arises between the total and partial elasticity of the grass cover. The definitions of total and partial elasticity are given in Section 3.3 and an example is shown in Figure 4.18. The analysis of the development of displacement and elasticity of the grass cover over successive loading cycles showed that the process of damage accumulation can be decomposed in three phases. The first phase is characterised by rapid increase of displacement and rapid decrease of elasticity. After the rapid increase of displacement, the second phase shows a displacement growth at a stable rate and

a slow and stable decrease of the elasticity of the specimen. During the third phase, the growth of displacement increases and elasticity of the test specimen decreases rapidly. The found process is consistent with the behaviour of other materials as described by (Li, 2013; Yang and Den Uijl, 2019). Because of the stable nature of the damage accumulation process in the second phase, the growth rate is a good measure of the accumulated damage. The same applies to the rate of decrease of elasticity. Based on the results of this study, the growth rate of the residual displacement is assumed to be determined by the magnitude of the induced load. However, the test results did not reveal whether the amplitude or the average value of the load is normative. Moreover, it remains unclear why the first load results in a relative large plastic deformation whereas, after the first load, the growth rate of the residual displacement has relatively small values.

6.2. Proposed method to determine grass cover parameter

The proposed method to estimate $\hat{S}_0$ provides a normative metric based on the physical processes that determine the resistance of grass covers against repetitive loads. This is a large improvement of assessments of the grass cover based on direct pull tests. Moreover, this relative simple and time efficient method provides a good estimation of the variability of the strength of the grass cover on a dike section. The method described by Bijlard et al. (2017) is based on a empirical relation between the maximum strength of the grass cover and the critical velocity u_c found in field test with the wave overtopping simulator. The critical velocity has theoretically the same physical meaning as the fatigue limit of the grass cover. Thereby, both methods provide a comparable strength metric of the grass cover. However, the proposed method enables to estimate a strength metric of the grass cover based on physical processes.

The proposed method to determine E and G is based on the prevailing literature and the findings of this study. Therefore it is reasonable to assume that the method provides reliable results. On the other hand, the method to determine k_s has a number of comments. The method is based on a fit of a solution of the one-dimensional consolidation problem to the results of a submerged stepwise increased constant load test. The utilized model describes one-dimensional consolidation. The model is based on the assumption that the time dependency of the deformation of the grass sod is completely attributed to drainage of negative pore pressure and the elasticity of the grass cover. This process is parametrized by constant values of E and k_s. During the execution of the stepwise increased constant load test, these assumptions are not valid. The pore water is not restricted to one direction, but is able to flow in all three directions. By only assuming one-dimensional drainage of negative pore water pressures, the values of k_s are overestimated. Nevertheless, in case of small deformations an approximation of k_s seems reasonable. Moreover, this attempt highlighted the possibilities to determine mechanical parameters based on tests with the grass sod pull device. Utilizing a more adequate model would already lead to large improvements.

6.3. Limitations of the study

The flaws during test execution made the test results unsuitable to determine a strength metric for the grass sod specimen subject to stepwise increased constant load and stepwise increased cyclic load. Due to the manual operation of the test device, the load history is different for each individual test. The resulting displacement is thereby a combined effect of the strength of the grass cover and the load history. Where the test results give a good indication of the occurring processes, the absolute values are not able to describe the strength of specific grass sod specimen. For the same reason, the test results did not give clear insights in the growth rate of the residual displacement. It remains unclear how the inclination of the trend line describing the growth rate of the residual displacement varies over the grass cover at one location. The test set-up showed imperfections as well. The set-up of the stepwise increased cyclic load regime did not allow to test the influence of the order of occurrence of loads with large magnitudes on damage accumulation.

6.4. Grass pull tests in relation with wave overtopping

The results of the pull tests revealed new insights into the mechanical behaviour. However, literature indicated that the resulting stress in the grass cover induced by overtopping waves is more complicated than stress perpendicular to the grass cover as induced with direct pull tests (Ponsioen, 2016; Schiereck, 2012; Valk, 2009; Van Damme et al., 2016; Van der Meer et al., 2012; Van Langevelde, 2017) . However, measurements showed that the strength of the grass sod parallel to the slope is a great deal larger than the strength in the direction perpendicular to the slope. Therefore, the strength in perpendicular direction is assumed to be normative for the mechanical behaviour of grass covers. Furthermore, pull tests reveal processes and mechanical behaviour of grass covers. These insights into the mechanical behaviour of the grass cover help to understand processes observed during wave overtopping. For example fatigue of the grass cover.

The occurrence of fatigue is consistent with observations during tests with the wave overtopping simulator that show that damage of the grass cover is a cumulative function of overtopping waves (Van der Meer et al., 2010). The relation between the load magnitude and the growth rate of the plastic deformation is in line with the theory that the contribute of individual waves to damage of the grass cover is a function of the size of the wave (Van der Meer et al., 2010). However, no threshold value for an excess load was found in this study.

7

Conclusions and Recommendations

The objective of this study was to gain a better understanding of the mechanical behaviour of grass covers under tensile load. To study this, field experiments were executed. This chapter presents the conclusions of this study by answering the research questions. Starting with:

1. **What are the physical processes and associated parameters that provide resistance of the grass cover against pull-out erosion induced by overtopping waves?**

The analysis of the test results show that deformation of grass covers due to tensile load is a time dependent process influenced by the degree of saturation. This indicates the occurrence of development and drainage of negative pore pressure associated with deformation of the grass cover due to tensile loading. The deformation process in not only determined by dissipation of pore pressure. Decrease of the grass cover elasticity under submerged conditions and ongoing deformation under a constant load indicate that other processes are involved as well.

This study showed that the load history of a grass cover has a negative influence on the pull out resistance. It was concluded that grass covers are subject to damage accumulation. Repetitive loading of the grass cover showed that part of the induced deformation can be identified as plastic and part as elastic. There was no stress level found that only resulted in elastic deformation. With an increasing number of successive load cycles, the portion of plastic deformation increases. The growth rate of the plastic deformation is related to the magnitude of the load. The elastic part of the deformation shows a stable decrease of stiffness up to failure of the grass cover. The decrease rate of the stiffness of the elastic part of the deformation is related to the magnitude of the load. Based on these findings, it is assumed that along with an increase in deformation, the material characteristics of the grass cover change. This results in a change of mechanical properties. In addition to the influence of the load, the degree of saturation is found to influence the failure process of the grass cover as well. Submerged conditions lead to higher portion of root failure due to slipping instead of breaking.

2. **What method can be used to measure the strength parameters?**

This study provided a lot of new insights into the mechanical behaviour of grass covers and has thereby improved the understanding of the mechanical behaviour of grass covers. Based on the new insights into mechanical behaviour of grass covers, a new method is proposed to assess resistance of grass covers against repetitive loading by means of direct pull test executed with the grass sod pull device.This relative simple and time efficient method enables to asses the erosion resistance of a grass cover on specific dike sections. The method is based on physical processes that determine the mechanical behaviour of the grass cover. The time efficiency of this method makes it feasible to test a large number of grass cover samples. Thereby, a good estimation of the variability of the strength of the grass cover on a dike section is provided by this method.

Engineering Recommendations

In order to assess the erosion resistance of large dike sections, it is advised to estimate the erosion resistance of the grass cover by direct pull tests as proposed in Chapter 5. This relative simple and time efficient method enables to asses the erosion resistance of a grass cover on specific dike sections based on physical processes that determine the mechanical behaviour of the grass cover. The time efficiency of this method makes it feasible to test a large number of grass cover samples. Thereby, a good estimation of the variability of the strength of the grass cover on a dike section is enabled by this method.

Research Recommendations

The results of the field tests provided insights into the occurring processes that influence the mechanical behaviour of grass covers under tensile load, but certain processes remain unknown. Especially insight in the progression of damage accumulation is missing. More insight in the growth rate of the plastic deformation is necessary to describe the process of damage accumulation in more detail. To gain more insights into the growth rate of the plastic deformation, the influence of the characteristics of the subsoil and the influence of the degree of saturation of the grass sod are of importance. As well as the influence of the order of occurrence of loads on the process of damage accumulation. The occurrence of fatigue of the grass cover implies that the order of occurrence of loads influence the moment of failure of the grass cover. However, the occurrence of fatigue does not imply that the progress of damage accumulation is influenced. The executed tests were not intended to study this effect. Therefore, this is a subject for further research. Furthermore, further research can reveal whether the value of E is influenced by the magnitude of the tensile load or if E is a function of time. In addition, more insights into the spatial variability of the strength of grass cover is desired. More test results enable to determine the number of required test in order to estimate probability density function of the grass cover strength.

Based on the findings of this study, recommendations for the execution of experiments with the purpose to determine the pull out resistance of the grass cover are made. First, it is advised to execute tensile test of the grass cover under submerged conditions in order to test the expected failure mode of the grass roots due to loading by overtopping waves. Second, a preparation of the grass cover specimen enabling to measure the strength only in one or in two directions is recommended to simplify the analysis of the test results. Furthermore the grass cover tensile test should be executed by a computer controlled device. Third, a difference between the perceived elasticity and the elasticity modulus E of the grass cover should be made.

List of Tables

List of Figures

List of Symbols

C	Degree of consolidation	$[-]$
E	Elasticity modulus	$[N/m^2]$
G	Shear modulus	$[N/m^2]$
N	Total number of cycles	$[-]$
S	Stress level	$[N/m^2]$
S_0	Fatigue limit	$[N/m^2]$
$\tilde{S}_0$	Estimated fatigue limit	$[N/m^2]$
U	Displacement	$[mm]$
U_{max}	Maximum displacement	$[mm]$
U_∞	Final displacement	$[mm]$
$\left(\frac{\Delta U}{N}\right)_{max}$	Maximum allowable growth rate	$[mm]$
c_v	consolidation coefficient	$[N/m^2]$
h	Half of layer of thickness of the sample	$[mm]$
n	Number of cycles	$[-]$
p	Pore water pressure	$[N/m^2]$
γ_w	Density of water	$[kg/m^3]$
Δ	Change of unit	$[-]$
γ	Deviatoric strain	$[-]$
ε	Strain	$[-]$
σ	Total stress	$[N/m^2]$
σ_{zz}	Total stress acting on plane normal to z, in the direction of z	$[N/m^2]$
$\sigma^{'}$	Effective stress	$[N/m^2]$

References

Bijlard, R.W. Strength of the grass sod on dikes during wave overtopping. Master of Science Thesis report, Delft University of Technology, 2015.

Bijlard, R.W., Steendam, G.J., H.J., Verhagen, and Van der Meer, J.W. Determining the critical velocity of grass sods for wave overtopping by a grass pulling device. Coastal Engineering Proceedings, 1 (35):20, 2017. ISSN 2156-1028. doi: 10.9753/icce.v35.structures.20. URL https://journals.tdl.org/icce/index.php/icce/article/view/8182.

Bomers, A. Road impact on erosion development during overtopping flood events. Master of Science Thesis report, University of Twente, 2015. URL http://essay.utwente.nl/67530/.

Cornelissen, H.A.W. Fatigue failure of concrete in tension. Heron, 29(4), 1984. URL https://www.scopus.com/inward/record.uri?eid=2-s2.0-0021620526&partnerID=40&md5=d9aee11e821f21a1dc19ecdd9776f127. cited By 46.

Cuomo, G., Lupoi, G., Shimosako, K., and Takahashi, S. Dynamic response and sliding distance of composite breakwaters under breaking and non-breaking wave attack. Coastal Engineering, 58 (10):953 – 969, 2011. ISSN 0378-3839. doi: https://doi.org/10.1016/j.coastaleng.2011.03.008. URL http://www.sciencedirect.com/science/article/pii/S0378383911000433.

Dean, R.G., Rosati, J.D., Walton, T.L., and Edge, B.L. Erosional equivalences of levees: Steady and intermittent wave overtopping. Ocean Engineering, 37(1):104 – 113, 2010. ISSN 0029-8018. doi: https://doi.org/10.1016/j.oceaneng.2009.07.016. URL http://www.sciencedirect.com/science/article/pii/S0029801809001796. A Forensic Analysis of Hurricane Katrina's Impact: Methods and Findings.

Hai, T.L. and Verhagen, H.J. Damage tograss covered slopes due toovertopping. volume 2014-January, 2014. URL https://www.scopus.com/inward/record.uri?eid=2-s2.0-84957692663&partnerID=40&md5=eeae73a772d73b6c9df7240159f455d5.

Hallett, P. D. and Newson, T. A. Describing soil crack formation using elastic–plastic fracture mechanics. European Journal of Soil Science, 56(1):31–38, 2005. doi: 10.1111/j.1365-2389.2004.00652.x. URL https://onlinelibrary.wiley.com/doi/abs/10.1111/j.1365-2389.2004.00652.x.

Helmons, R.L.J. and Van Rhee, C. A 3d method to dynamically model the cutting of submerged rocks with evaluation of pore pressure effects. pages 136–146, 2019. URL https://www.scopus.com/inward/record.uri?eid=2-s2.0-85071427816&partnerID=40&md5=bcf527c4d71c8b1c8ed29945e6526e59.

Hoffmans, G., Akkerman, G.J., Verheij, H., Van Hoven, A., and Van Der Meer, J. The erodibility of grassed inner dike slopes against wave overtopping. pages 3224–3236, 2009. URL https://www.scopus.com/inward/record.uri?eid=2-s2.0-84873849415&partnerID=40&md5=a1e56f8dc37d76e87b1d715d54d39b32.

Hoffmans, G.J.C.M. The influence of turbulence on soil erosion, volume 10. Eburon Uitgeverij BV, 2012.

Kok, M., Vrijling, J.K., and Zevenbergen, C. Towards an integrated evaluation framework for multifunctional flood defences. Comprehensive Flood Risk Management. Taylor & Francis Group, London, pages 921–926, 2013.

Kortenhaus, A. Probabilistische Methoden für Nordseedeiche. PhD thesis, PhD thesis,Technischen Universität Carolo-Wilhelmina zu Braunschweig, 2003.

Li, Jian, Tang, Chaosheng, Wang, Deying, Pei, Xiangjun, and Shi, Bin. Effect of discrete fibre reinforcement on soil tensile strength. Journal of Rock Mechanics and Geotechnical Engineering, 6(2):133 – 137, 2014. ISSN 1674-7755. doi: https://doi.org/10.1016/j.jrmge.2014.01.003. URL http://www.sciencedirect.com/science/article/pii/S1674775514000122.

Li, Ning. Asphalt mixture fatigue testing: Influence of test type and specimen size. 2013.

Muijs, J.A. Grass cover as a dike revetment, translation of taw- brochure 'grasmat als dijkbekleding' 9. DWW report, 1999.

Pijpers, R. Vulnerability of structural transitions in flood defences: Erosion of grass covers due to wave overtopping. Master of Science Thesis report, Delft University of Technology, 2013.

Pollen, N. Temporal and spatial variability in root reinforcement of streambanks: accounting for soil shear strength and moisture. Catena, 69(3):197–205, 2007.

Ponsioen, L., Van Damme, M., Hofland, B., and Peeters, P. Relating grass failure on the landside slope to wave overtopping induced excess normal stresses. Coastal Engineering, 148:49 – 56, 2019. ISSN 0378-3839. doi: https://doi.org/10.1016/j.coastaleng.2018.12.009. URL http://www.sciencedirect.com/science/article/pii/S0378383917303642.

Ponsioen, L.A. Overflow and wave overtopping induced failure processes on the land-side slope of a dike. Master of Science Thesis report, Delft University of Technology, 2016.

Roylance, D. Module 24: Fatigue. In Mechanics of Materials—MIT Course No. 3.11. Cambridge MA, 2001a. URL https://ocw.mit.edu/courses/materials-science-and-engineering/3-11-mechanics-of-materials-fall-1999/modules/. MIT OpenCourseWare.

Roylance, D. Module 23: Introduction to fracture mechanics. In Mechanics of Materials—MIT Course No. 3.11. Cambridge MA, 2001b. URL https://ocw.mit.edu/courses/materials-science-and-engineering/3-11-mechanics-of-materials-fall-1999/modules/. MIT OpenCourseWare.

Schiereck, G.J. Introduction to bed, bank and shore protection (HJ Verhagen ed. Delft: VSSD, 2012.

Schüttrumpf, H. and Oumeraci, H. Layer thicknesses and velocities of wave overtopping flow at seadikes. Coastal Engineering, 52(6):473 – 495, 2005. ISSN 0378-3839. doi: https://doi.org/10.1016/j.coastaleng.2005.02.002. URL http://www.sciencedirect.com/science/article/pii/S0378383905000232.

Schüttrumpf, H. and Van Gent, M.R. A. Wave overtopping at seadikes. In Coastal Structures 2003, pages 431–443. 2003. doi: 10.1061/40733(147)36.

Sprangers, J. Vegetation dynamics and erosion resistance of sea dyke grassland. PhD thesis, PhD thesis, Wageningen Agriculture University, 1999.

Stanczak, G. and Oumeraci, H. Modeling sea dike breaching induced by breaking wave impact-laboratory experiments and computational model. Coastal Engineering, 59(1):28 – 37, 2012. ISSN 0378-3839. doi: https://doi.org/10.1016/j.coastaleng.2011.07.001. URL http://www.sciencedirect.com/science/article/pii/S0378383911001219.

Steendam, G.J., Provoost, Y., and Van der Meer, J.W. Destructive wave overtopping and wave run-up tests on grass covered slopes of real dikes. Coastal Engineering Proceedings, 1(33):64, 2012. ISSN 2156-1028. doi: 10.9753/icce.v33.structures.64. URL https://journals.tdl.org/icce/index.php/icce/article/view/6932.

Steendam, G.J., Van Hoven, A., Van der Meer, J., and Hoffmans, G. Wave overtopping simulator tests on transitions and obstacles at grass covered slopes of dikes. Coastal Engineering Proceedings, 1 (34):79, 2014. ISSN 2156-1028. doi: 10.9753/icce.v34.structures.79. URL https://journals.tdl.org/icce/index.php/icce/article/view/7965.

Takken, W., van Vliet, A.J.H., Verhagen, A., and Vos, C.C. Wegen naar een klimaatbestendig Nederland. Planbureau voor de Leefomgeving, 2009.

Terzaghi, K and Peck, R.B. Soil mechanics in engineering practice. 1948.

Tollenaar, R.N., van Paassen, L.A., and Jommi, C. Experimental evaluation of the effects of pull rate on the tensile behavior of a clay. Applied Clay Science, 144:131 – 140, 2017. ISSN 0169-1317. doi: https://doi.org/10.1016/j.clay.2017.04.026. URL http://www.sciencedirect.com/science/article/pii/S0169131717301898.

Valk, A. Wave overtopping: Impact of water jets on grassed inner slope transitions. Master of Science Thesis report, Delft University of Technology, 2009.

Van Damme, M. Distributions for wave overtopping parameters for stress strength analyses on flood embankments. Coastal Engineering, 116:195 – 206, 2016. ISSN 0378-3839. doi: https://doi.org/10.1016/j.coastaleng.2016.06.010. URL http://www.sciencedirect.com/science/article/pii/S0378383916301211.

Van Damme, M. Personal correspondence with Dr. ir. M. van Damme postdoctoral researcher for Hydraulic structures and Flood risk at TU Delft. 2019.

Van Damme, M., Ponsioen, L.A., Herrero Huerta, M., and Peeters, P. Comparing overflow and wave-overtopping induced breach initiation mechanisms in an embankment breach experiment. Flood Risk 2016, 7, 2016.

Van der Meer, J, Verheij, H, Hoffmans, G, Paulissen, MPCP, Steendam, GJ, and van Hoven, A. Technisch rapport toetsen grasbekledingen op dijken. Technical report, Deltares, 2012.

Van der Meer, J.W., Bernardini, P., Snijders, W., and Regeling, E. The wave overtopping simulator. In Coastal Engineering 2006: (In 5 Volumes), pages 4654–4666. World Scientific, 2006.

Van Der Meer, J.W., Bernardini, P., Steendam, G.J, Akkerman, G.J, and Hoffmans, G.J.C.M. The wave overtopping simulator in action. In Coastal Structures 2007: (In 2 Volumes), pages 645–656. World Scientific, 2007.

Van der Meer, J.W., Hardeman, B., Steendam, G.J., Schuttrumpf, H., and Verheij, H.J. Flow depths and velocities at crest and inner slope of a dike, in theory and with the wave overtopping simulator. Coastal Engineering Proceedings, 1(32):10, 2010. ISSN 2156-1028. doi: 10.9753/icce.v32.structures.10. URL https://icce-ojs-tamu.tdl.org/icce/index.php/icce/article/view/1239.

Van der Meer, J.W., Van Hovern, A., Paulissen, M., Steendam, G.J., Verheij, H.J., Hoffmans, G.J.C.M., and Kruse, G. Handreiking dijkbekledingen deel 5: Grasbekledingen. 2015.

Van Langevelde, A.B. 2D modelling of initiation of failure of a clay slope under wave overtopping load. Master of Science Thesis report, Delft University of Technology, 2017.

Van Ooijen, D.C. Technical report clay for dikes. English translation of a TAW-guideline, 1996.

Verheij, H.J., Kruse, G.A.M., Niemeijer, J.H., Sprangers, J.T.C.M., De Smidt, J.T., and Wondergem, P.J.M. Technical report erosion resistance of grassland as dike covering. English translation of a TAW guideline, 1997.

Verheij, H.J., Hoffmans, G.J.C.M., and Van der Meer, J.W. Evaluation and Model Development; Grass Erosion Test at the Rhine dike. Technical report, Deltares, 2015.

Verruijt, A. Soil Mechanics. 2007.

Verruijt, A. An Introduction to Soil Dynamics. 01 2010. doi: 10.1007/978-90-481-3441-0.

Winterwerp, J.C. and Van Kesteren, W.G.M. Introduction to the Physics of Cohesive Sediment in the Marine Environment, volume 56 of Developments in Sedimentology. Elsevier, 2004. doi: https://doi.org/10.1016/S0070-4571(04)80009-8. URL http://www.sciencedirect.com/science/article/pii/S0070457104800098.

Yang, Y and Den Uijl, J.A. Part on Concrete and Concrete Structures. Lecture Notes of Fatigue CIE5126. Delft University of Technology, 2019.

A

Erosion models

Various models are developed to describe the erosion process of grass covers under wave overtopping flows. The empirical erosion limits considered in the erosion models are based on observations during wave overtopping experiments. Dean et al. (2010) considered three possible three physical bases for erosion, which in essence can be described as follows:

$$\text{Velocity above a threshold value:} \quad E = \sum_{i=1}^{N_c} K\Big(U_i - U_c\Big)t \tag{A.1}$$

$$\text{Shear stress above a threshold value:} \quad E = \sum_{i=1}^{N_c} K\Big({U_i}^2 - {U_c}^2\Big)t \tag{A.2}$$

$$\text{Work above a threshold value:} \quad E = \sum_{i=1}^{N_c} K\Big({U_i}^3 - {U_c}^3\Big)t \tag{A.3}$$

E is the amount of erosion which sums over the number of waves N_c for which holds $U_i > U_c$. K is a group factor of all unknown coefficients. In all three bases is assumed that only loading above a threshold value will contribute to erosion. This method does not only describe the erosion process, it result as well in a strength parameter of the grass cover. In this way U_c is formulated as a measure of the strength of the grass cover loaded by overtopping waves.

Van der Meer et al. (2010) performed overtopping experiments on real dikes and observed indeed that only waves of a certain volume (or velocity) damaged the slope. Smaller volumes did not contribute to the development of damage. This confirms the use of a threshold, like U_c. Furthermore Van der Meer et al. (2010) found that erosion was caused by the impact of the maximum flow velocity during a short time period within the overtopping duration. For this reason, the overtopping duration can be omitted. This results in a erosional index called the cumulative hydraulic load D as formulated in Equation A.4

$$D = \sum_{i=1}^{N_c} \Big({U_i}^2 - {U_c}^2\Big) \tag{A.4}$$

The cumulative hydraulic load can be coupled to damage criteria as described by Van der Meer et al. (2010) and Steendam et al. (2012). The hydraulic load is separated in three erosion categories:

$$\text{Initial damage:} \quad D < 500 m^2/s^2$$

$$\text{Damage at various locations:} \quad 500 m^2/s^2 < D < 1500 m^2/s^2$$

$$\text{Failure of dike slope:} \quad D > 3500 m^2/s^2$$

However, field experiments showed that is hard to determine the precise erosion category of a slope during wave overtopping. The criterion failure is most clear to determine.

The damage indication, according to the Cumulative overload method, can be seen as inversely proportional to the erosion resistance or strength of the grass cover. Assuming loading by waves of the same magnitude result in a constant growth of the damage, and a constant decrease of the strength by applying the Cumulative overload method.

B

Empirical method to determine the critical velocity of grass sods for wave overtopping by a grass pulling device

To investigate the strength of a grass covers on dikes, a device developed by Infram B.V. in cooperation with Van der Meer Inovations. The grass pulling device is able to measure the strength of the grass sod in situ. While lifting the grass sod perpendicular to the slope out of the sod with the grass pulling device the imposed force is measured. This device is originally developed to fit the Cumulative Overload Method developed by Van der Meer et al. (2010). Bijlard (2015; 2017) used the Turf-element model (Hoffmans et al., 2009) to find a relation to express the lifting force into the critical flow velocity that can be used as indication of the strength of the grass cover of the dike.

The test set-up of the sod pulling test consists of a small pull frame with demensions of $20x20cm^2$ (Figure B.1 a), which is pulled up by a hydraulic cylinder and a manually operated hydraulic pump. The cylinder is placed in a supporting frame, which is placed directly above the small pull frame (Figure B.1. The tensile forces is measured by applying a force measuring sensor. In order to place the pull frame, the soil has to be excavated on two opposite sides up to 8 cm depth. Five pins are inserted below the surface of the grass through the soil in the frame.

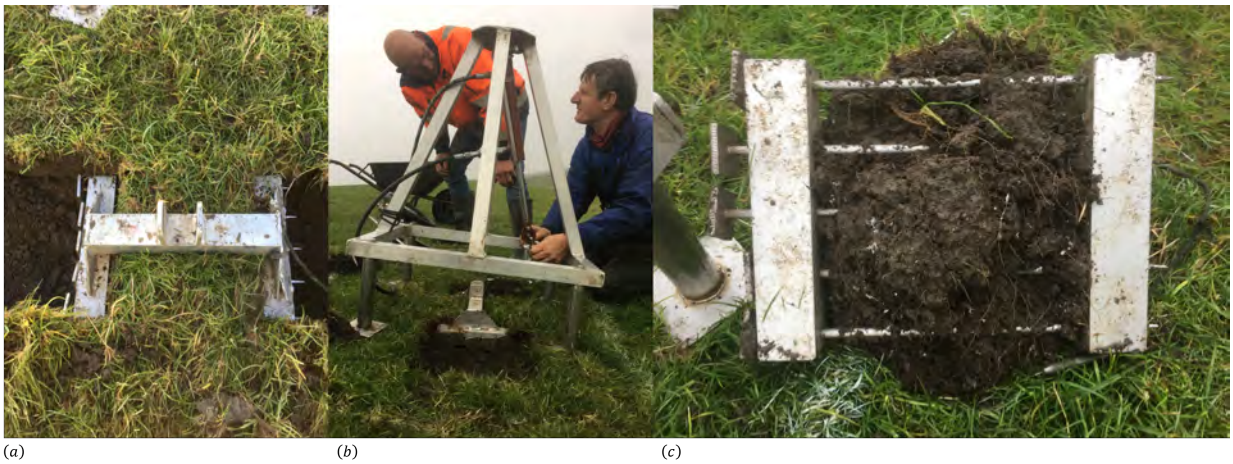

(a) (b) (c)

Figure B.1: The test set-up of the sod pulling test with pull frame and supporting frame Source :Own pictures November 2018.

The sod pulling can be preformed with two conditions during pulling. The tests are performed with two sides of the sod cut and two sides intact (condition 2 test) and with all four sides cut loose (condition 4 test). With this last test the sides do not contribute to the measured strength during lifting of the sod, only the bottom of the sod resists against the uplifting force. The condition 2 test is mostly applied. The sod conditions can also be a variable during testing. The ground is not completely saturated under

normal conditions, but during storms (which can result in overtopping waves) the ground will become more and more saturated over time. In order to mimic the conditions during wave overtopping as much as possible, the ground should be saturated for some time before testing begins.

The sod is pulled out with a constant increasing displacement of $1cm/sec$. critical mean grass normal stress can be determined by Equation B.1.

$$\sigma_{grass,c} = \frac{F_i}{A_b + 4A_s} \tag{B.1}$$

With $\sigma_{grass,c}$ Critcal mean grass normal stress, F_i Maximum pulling force, A_b Bottom area pulled out sod and A_s Side area pulled out sod. The critical flow velocity (U_c)can be calculated with Equation B.2 (Bijlard, 2015)

$$U_c = \alpha_{grass,u} r_0^{-1} \sqrt{\frac{\Psi_c(\sigma_{grass,c} - p_w}{\rho}} \tag{B.2}$$

In the above equation r_0^{-1} is the relative turbulence of the overtopping wave over the slope.Ψ_c is the Shields parameter for transport of soil under flow velocities. $\sigma_{grass,c}$ is the critical normal stress of the grass sod determined with the sod pulling tests. The pore water pressure (or suction pressure) is given as p_w, which increases the strength of the unsaturated soil. The suction pressures should be overcome before the grass sod can be lifted up. The density of the water is given by ρ and $\alpha_{grass,u}$ is a constant with the value of 2.0.

The critical flow velocity (U_c) can be used as indication of the grass cover strength under wave loading. The Cumulative Overload Method developed by Van der Meer et al. (2010). This theory considers failure of a dike due to wave overtopping. According to this theory, the water flow imposes a load to the dike cover during overtopping. If the load excesses a certain threshold or critical value, failure of the dike cover is expected. Therefore the flow velocity is assumed to be the normative factor to induce failure of the dike cover. Therefore, the critical flow velocity can be seen as a strength parameter.